HHS Public Access

Author manuscript

Cell. Author manuscript; available in PMC 2019 October 18.

Published in final edited form as:

Cell. 2018 October 18; 175(3): 809–821.e19. doi:10.1016/j.cell.2018.08.046.

Protein AMPylation by an evolutionarily conserved pseudokinase

Anju Sreelatha[1], **Samantha S. Yee**[1,9], **Victor A. Lopez**[1], **Brenden C. Park**[1], **Lisa Kinch**[2], **Sylwia Pilch**[3], **Kelly A. Servage**[1], **Junmei Zhang**[1,10], **Jenny Jiou**[2], **Monika Karasiewicz**[3], **Małgorzata Łobocka**[3,4], **Nick Grishin**[2,5], **Kim Orth**[1,5,6], **Roza Kucharczyk**[3], **Krzysztof Pawłowski**[6], **Diana R. Tomchick**[2,6], and **Vincent S. Tagliabracci**[1,7,8,11,*]

[1]Department of Molecular Biology, University of Texas Southwestern Medical Center, Dallas, TX 75390, USA. [2]Department of Biophysics, University of Texas Southwestern Medical Center, Dallas, TX 75390, USA. [3]Institute of Biochemistry and Biophysics, Polish Academy of Sciences, Warsaw 02-106, Poland. [4]Faculty of Agriculture and Biology, Warsaw University of Life Sciences, Warsaw 02-787, Poland [5]Howard Hughes Medical Institute, Dallas, TX 75390, USA. [6]Department of Biochemistry, University of Texas Southwestern Medical Center, Dallas, TX 75390, USA. [7]Harold C. Simmons Comprehensive Cancer Center, University of Texas Southwestern Medical Center, Dallas, Texas 75390, USA [8]Hamon Center for Regenerative Science and Medicine, University of Texas Southwestern Medical Center, Dallas, Texas 75390, USA [9] Current address: Department of Pharmacology, The University of Texas Health Science Center at San Antonio, San Antonio, Texas 78229-3900, United States [10] Current address: Department of Pharmaceutical Sciences, School of Pharmacy, University of Pittsburgh, Pittsburgh, PA 15261, USA. [11]Lead Contact

Summary

Approximately 10% of human protein kinases are believed to be inactive and named pseudokinases because they lack residues required for catalysis. Here we show that the highly conserved pseudokinase selenoprotein-O (SelO) transfers AMP from ATP to Ser, Thr and Tyr residues on protein substrates (AMPylation), uncovering a previously unrecognized activity for a member of the protein kinase superfamily. The crystal structure of a SelO homolog reveals a protein kinase-like fold with ATP flipped in the active site, thus providing a structural basis for catalysis. SelO pseudokinases localize to the mitochondria and AMPylate proteins involved in redox homeostasis. Consequently, SelO activity is necessary for the proper cellular response to oxidative stress. Our results suggest that AMPylation may be a more widespread post translational modification than previously appreciated and that pseudokinases should be analyzed for alternative transferase activities.

*Correspondence: Vincent S. Tagliabracci (vincent.tagliabracci@utsouthwestern.edu).

Author contributions

A.S. and V.S.T. designed the experiments. A.S, S.S.Y, V.A.L., B.C.P, S.P., J.J., M.K., M.L., R.K., D.R.T. and V.S.T conducted the experiments. J.Z. and K.A.S. performed the mass spectrometry. L.K, N.G, and K.P. performed the bioinformatics. M.L and K.O. provided essential reagents. A.S., L.K., K.P., and V.S.T wrote the manuscript with input from all authors.

Declaration of Interests

The authors declare no competing interests.

Keywords

adenylylation; kinase structure; oxidative stress; selenocysteine; SELENOO; glutathionylation; glutaredoxin

Introduction

Protein kinases are an important class of enzymes that transfer phosphate from ATP to protein substrates, a process known as phosphorylation (Fischer, 2013). Virtually every cellular activity is regulated by protein kinases, and abnormal phosphorylation has been linked to numerous diseases. More than 500 human protein kinases have been identified and assembled into an evolutionary tree known as the human “kinome” (Manning et al., 2002). However, research is largely biased toward kinases with well-established roles in disease; it has been estimated that the molecular functions of more than 50% of human kinases remain uncharacterized (Fedorov et al., 2010). Furthermore, several new kinase families have been identified that are so different, they were not included on the human kinome tree. These include the Fam20 and Fam69 families of secretory pathway kinases (Dudkiewicz et al., 2013; Tagliabracci et al., 2012) and the selenocysteine (Sec)-containing protein Selenoprotein-O (SelO) (Dudkiewicz et al., 2012).

About 10% of human protein kinases are predicted to be inactive and referred to as pseudokinases because they are missing residues located in highly conserved sequence motifs believed to be required for ATP binding and catalysis (Manning et al., 2002). Pseudokinases serve a multitude of non-catalytic roles, such as allosteric regulators or scaffolding functions (Eyers and Murphy, 2013; Kung and Jura, 2016; Taylor et al., 2013; Zeqiraj and van Aalten, 2010). For example, the Fam20A pseudokinase binds to and increases the stability and activity of the secretory pathway kinase Fam20C, thus acting as an allosteric regulator (Cui et al., 2015). Similarly, the HER3 pseudokinase, although reported to have low catalytic activity, serves mostly as an allosteric activator for other members of the EGFR family of receptor kinases (Jura et al., 2009; Shi et al., 2010). These studies have highlighted the importance of pseudokinases in human biology and their diverse signaling functions make them attractive drug targets (Bailey et al., 2015; Byrne et al., 2017).

Pseudokinases were initially predicted to be inactive if they were missing one or more of the three critical residues known to participate in phosphotransfer in active kinases (Manning et al., 2002). These include **1)** the VAIK motif in the β3-strand, where the Lys positions the α and β phosphates of ATP for catalysis (K72 using protein kinase A; PKA nomenclature) **2)** the HRD motif located in the catalytic loop, where the Asp acts as the catalytic base (PKA; D166) and **3)** the DFG motif; where the Asp binds the divalent cation to coordinate the β and γ phosphates of ATP (PKA; D184). However, some predicted pseudokinases have evolved compensatory mechanisms to catalyze phosphorylation by migration of active site residues including the WNK family of kinases (Min et al., 2004) and the protein O-mannosyl kinase, SGK196 (Zhu et al., 2016). Such compensatory mutations are often

difficult to identify by primary amino acid sequence alone and have resulted in the wrongful annotation of some kinases as inactive.

We previously predicted SelO to adopt a protein kinase fold (Dudkiewicz et al., 2012). However, its sequence suggests that SelO would be an inactive pseudokinase because it lacks the catalytic Asp (PKA; D166) (Figures 1A and S1). Human SelO localizes to the mitochondria and incorporates the 21st genetically encoded amino acid selenocysteine (Sec) (Han et al., 2014; Kryukov et al., 2003). Structurally, Sec is similar to Cys but contains a selenium atom in place of sulfur (Stadtman, 1974). The resulting selenol group has a lower pKa than the sulfur-containing thiol group and is deprotonated at physiological pH, resulting in higher nucleophilicity and oxidoreductase efficiency (Labunskyy et al., 2014). Twenty-five selenoproteins are encoded in the human genome and many are involved in cellular redox homeostasis (Kryukov et al., 2003). In higher eukaryotes, most SelO homologs contain a single Sec near the carboxy terminus (Han et al., 2014; Kryukov et al., 2003). In lower eukaryotes and all prokaryotes containing a SelO homolog, an invariant Cys occupies the equivalent position (Figure 1B). For simplicity, we will use the SelO name for the entire family regardless of whether or not the protein contains a Sec.

SelO is highly conserved, having homologs widespread among most eukaryotic taxa and is also common in many major bacterial taxa (Dudkiewicz et al., 2012). Despite this sequence-based indicator of a universal role across kingdoms, the molecular function of SelO is unknown. In fact, when prioritizing targets for experimental study, Koonin and colleagues listed SelO among the top ten most-attractive “unknown unknowns” because of phyletic spread and potential to reveal new and exciting biology (Galperin and Koonin, 2004).

Here we report the crystal structure of a SelO homolog, which reveals a protein kinase-like fold. Remarkably, the ATP in the active site is flipped relative to the orientation of ATP in the active site of canonical kinases. Our structural studies led us to discover that the SelO pseudokinases are in fact active enzymes, yet transfer AMP, instead of a phosphate group, to Ser, Thr and Tyr residues on protein substrates (AMPylation aka adenylylation). Furthermore, we uncover that SelO plays an evolutionarily conserved role in the cellular response to oxidative stress by AMPylating proteins involved in redox homeostasis. We anticipate that the results of this work will have important implications for redox biology and may have the potential to define new paradigms of cellular regulation and signal transduction.

Results

SelO is one of the most highly conserved members of the protein kinase and selenoprotein families

To demonstrate the unique conservation of SelO, we performed basic local alignment search tool (BLAST) analyses against the Representative Proteomes RP55 database limited to bacteria using known human kinase domains and selenoproteins as queries in the search. We represent conservations of these different kinase and selenoprotein families as a plot of E-value vs. sequence identity of the top bacterial protein returned from the search (Figure 1C). Our results indicate that SelO is one of the most highly conserved members of either the

human protein kinase families or the various selenoprotein families. Among bacteria, SelO is ubiquitous in Proteobacteria and Cyanobacteria while in other phyla it is less frequent. Among eukaryotes, in most phyla there is on average one SelO gene per genome, while chordates and arthropods are exceptions, having an average of two or 0.14 genes per genome, respectively.

SelO adopts a protein kinase fold with ATP flipped in the active site

To gain insight into the function of the SelO pseudokinases, we solved the crystal structure of the SelO homolog from the gram-negative plant pathogen *Pseudomonas syringae* bound to an ATP derivative AMP-PNP (Figures 2A, S2A & Table S1). Despite the unique sequence found in the SelO family, *P. syringae* SelO adopts a protein kinase-like fold consisting of 12 β-strands and 22 α-helices, with the kinase domain identifying a number of kinase structures as top hits using DALI or VAST structural homology searches engines (i.e. aerobactin synthase IucA, the plant receptor kinase BRASSINOSTEROID INSENSITIVE 1, the human interleukin-1 receptor-associated kinase 4, and tyrosine kinase Syk). The kinase core (β4-α14) consists of a β-strand-rich N-lobe and an α-helical-rich C-lobe connected by a flexible linker that can be superimposed onto protein kinase CK1 with a root mean square derivation (rmsd) of 3.5 Å over 164 Cα atoms (Figure S2B). The SelO N-lobe includes the regulatory αC helix (Figure 2A, orange) packing against the core β-sheet (Figure 2A, magenta), while the C-lobe includes a pseudo-catalytic loop lacking HRD, followed by an apparent activation loop. An N-terminal extension (α1-α5, white) stabilizes the N-lobe β-sheet, and the unique C-terminal domains, CTD1 (α15-α19) and CTD2 (α20-α22), contact the C-lobe and the αC helix, respectively. There is no clear electron density for the last 12 residues, including the C-terminal Cys/Sec, suggesting that this region is disordered.

The SelO nucleotide sits in a cleft between the two lobes of the kinase domain. Remarkably, the AMP-PNP molecule is flipped in the active site when compared to canonical protein kinases. The γ-phosphate, which is normally transferred to protein in a kinase reaction, is buried in a pocket between the two lobes of the kinase domain (Figure 2B). In fact, after superposition of the kinase domains, the SelO α, β, and γ-phosphates occupy the positions of the typical γ, β, and α-phosphates of protein kinases, respectively (Figures 2B, 2C and S2C). The binding site for the flipped nucleotide adenine base and sugar ribose is formed by unique insertions in two SelO loops: the β6-β7 (Gly-rich loop) and the β8-αC loop (colored white, Figures 2B and D).

SelO transfers AMP from ATP to protein substrates

The flipped orientation of ATP in the active site led us to hypothesize that the SelO proteins could transfer adenosine monophosphate (AMP) to protein substrates (AMPylation) (Casey and Orth, 2017). We incubated recombinant *E. coli* (ydiU), *S. cerevisiae* (Fmp40) and *H. sapiens* SelO with [γ^{32}P]ATP or [α^{32}P]ATP of similar specific radioactivity and observed ^{32}P-incorporation into the WT proteins only when [α^{32}P]ATP was used as substrate (Figures 3A, B, C). Mutation of the active site metal binding DFG motif in the SelO proteins abolished ^{32}P incorporation. *E. coli* and human SelO, but not the inactive mutants, were immunoreactive to an anti-Thr AMP antibody (Figures S3A and S3B) (Hao et al., 2011). Likewise, mass spectrometry (MS) analysis revealed tryptic peptides from WT SelO proteins

but not the inactive mutants, with mass shifts of 329 Da, consistent with the covalent addition of AMP to Ser, Thr and Tyr residues (Figure 3D and S3C). Furthermore, *E. coli* SelO, but not the inactive mutant, could AMPylate the generic protein kinase substrate myelin basic protein (MBP) in a time dependent manner (Figure 3E). *E. coli* SelO prefers ATP over other nucleotides as a co-substrate (Figure S3D) and displayed a K_m for ATP of ~2.0 μM (Figure S3E). Thus, the SelO pseudokinases can AMPylate protein substrates.

Unique interactions within the SelO active site facilitate nucleotide binding and AMPylation

Several interactions within the SelO active site contribute to the inverted orientation of the nucleotide, including K113 (PKA K72) that coordinates the γ-phosphate of ATP (Figure 4A). K113 extends into the active site and is stabilized by E136 from the α6/αC helix. The formation of this ion pair, which typically positions the α-phosphate of ATP, is considered a hallmark of the activated state of a protein kinase (Taylor and Kornev, 2011). Two invariant arginines (R176 and R183) also form interactions with the γ-phosphate. R176 extends into the active site from β12 and R183 lies in the flexible hinge region that connects the N-lobe to the C–lobe (Figure 4A). Mutations of K113, E136, R176 or R183 to Ala inactivate *E. coli* SelO (Figure 4B). Most kinases require a divalent cation to orient the phosphates of ATP. In the *P. syringae* SelO structure, Mg^{2+} and Ca^{2+} are bound to the α and β phosphates of AMP-PNP and are coordinated by N253 and D262 (PKA N171 and D184). Mutations of these residues to Ala abolished *E. coli* SelO activity (Figure 4B). SelO was predicted to be a pseudokinase because it lacks the catalytic Asp (PKA D166), which deprotonates the phosphoacceptor hydroxyl on the protein substrate. However, we anticipate that D252 in *P. syringae* SelO could fulfill this role because of its conservation, its proximity to the α-phosphate of ATP and when mutated to Ala, the enzyme is inactive. Collectively, the active site of *P. syringae* SelO reveals evolutionarily conserved interactions that provide this family of kinases with the unique ability to transfer AMP to protein substrates.

SelO is a redox active mitochondrial protein

The N-terminus of eukaryotic SelO proteins contains a predicted mitochondrial targeting peptide (mTP). When overexpressed in mammalian cells as a GFP-fusion protein, human SelO localizes to the mitochondria (Han et al., 2014). We expressed *S. cerevisiae* SelO (official gene name *Fmp40*) in yeast as a C-terminally tagged GFP fusion protein and observed co-localization with the mitochondrial resident protein citrate synthase (Figure S4A). Mitochondrial localization was dependent on the presence of the mTP (residues 1–23) because a truncated mutant of SelO failed to localize to the mitochondria (Figure S4A). Furthermore, we fractionated yeast extracts by sucrose gradient centrifugation and detected endogenous SelO in fractions enriched for the mitochondrial resident protein porin (Figure S4B). Thus, *S. cerevisiae* SelO is a mitochondrial protein and its localization depends on a functional mTP.

Many mitochondrial proteins are subjected to redox regulation, including several selenoproteins. To test the redox function of SelO, we purified the *E. coli* protein under non-reducing conditions and observed a doublet when the protein was resolved by non-reducing SDS PAGE (Figure 5A). The faster migrating species was converted to the slower migrating

species upon treatment with the reducing agent dithiothreitol (DTT). Likewise, endogenous *S. cerevisiae* SelO migrated as two distinct species during non-reducing SDS PAGE and was also sensitive to DTT (Figure 5B). MS analysis of *E. coli* SelO identified an intramolecular disulfide bond between Cys272 and Cys476 (Figure 5C). To confirm the sites of modification, we incubated *E. coli* SelO with the cysteine alkylating agent 4-acetamido-4′-maleimidylstilbene-2,2′-disulfonic acid (AMS). AMS reacts with free thiols resulting in a change in electrophoretic mobility that can be easily observed by SDS PAGE. AMS reduced the electrophoretic mobility of WT SelO, only in the presence of the reducing agent, Tris(2-carboxyethyl) phosphine (TCEP). However, AMS reduced the electrophoretic mobility of the C272A and C476A mutants in the absence of TCEP (Figure 5D). Collectively, these results suggest that *E. coli* SelO forms an intramolecular disulfide bond between a Cys in the activation loop and the Cys at the C-terminus, the latter being replaced by a Sec in higher eukaryotes (Figures 1A and 5E).

The formation of disulfide bonds occurs primarily in the oxidizing environment of the secretory pathway. However, some mitochondrial proteins can also form disulfide or selenyl-sulfide bonds as part of their catalytic mechanism (Collet and Messens, 2010). To test whether the SelO disulfide bond regulates its activity, we incubated *E. coli* SelO purified under non-reducing conditions, with MBP and [α^{32}P]ATP and observed low levels of AMPylation (Figure 5F). However, addition of DTT or the thioredoxin system that uses reducing equivalents from NADPH to reduce disulfides, markedly increased SelO activity. Therefore, *E. coli* SelO activity is regulated by the formation of an intramolecular disulfide bridge.

SelO AMPylates proteins involved in redox biology

Based on the chemistry of the AMPylation reaction and the location of the adenine ring of ATP in the SelO crystal structure, we reasoned that using a biotinylated ATP analog would be an efficient strategy to identify proteins AMPylated by SelO. In this reaction, biotinylated AMP would be transferred to proteins, which would greatly facilitate isolation and identification of SelO substrates. We incubated *E. coli* SelO with Biotin-17-ATP (Figure 6A) and *E. coli* extracts (Figure 6B). Remarkably, several biotinylated proteins were observed in extracts incubated with WT SelO but not the inactive mutant. To identify SelO targets, we enriched biotinylated proteins by avidin pulldown and identified potential SelO substrates by mass spectrometry, several of which have roles in oxidative phosphorylation and redox biology (Table S2). Among our top candidates are sucA, the bacterial homolog of the E1 component of the alpha-ketoglutarate dehydrogenase complex (Frank et al., 2007) and glutaredoxin (grx), a small thioredoxin-like protein that catalyzes the removal of covalently linked glutathione from Cys residues on proteins (de-glutathionylation) (Shelton et al., 2005).

To test whether *E. coli* sucA and grxA are AMPylated by SelO in cells, we co-expressed *E. coli* SelO or the inactive mutant with His-tagged sucA or grxA and analyzed Ni-NTA affinity purified proteins for AMPylation by mass spectrometry. We identified AMPylated tryptic peptides on sucA and grxA that were present when co-expressed with WT but not inactive SelO (Figures S5). Notably, we identified Thr405 on sucA and Tyr13 on grxA to be

potential sites of modification. Protein immunoblotting of sucA using an anti-Thr AMP antibody confirmed Thr405 was the major site of AMPylation (Figure 6C). Likewise, SelO AMPylated WT grxA *in vitro* but not the Y13F mutant (Figure 6D). Thus, SelO can AMPylate Thr and Tyr residues on protein substrates both *in vitro* and *in vivo*.

To determine the substrate specificity of SelO, we performed AMPylation reactions using *E. coli* grxA as a model substrate. Alanine substitutions of the Cys at the −2 and Pro at the −1 positions, or replacing the AMP-acceptor Tyr with a Ser or a Thr, markedly inhibited SelO-mediated AMPylation (Figure S6A). However, analysis of the auto AMPylation sites in *E. coli*, yeast and human SelO (Figure S3C), and the grxA and sucA sites (Figure S5), did not reveal any obvious primary sequence requirements for SelO-catalyzed AMPylation. Therefore, SelO appears to require additional factors beyond the primary amino acid sequence of the substrate.

SelO-mediated AMPylation protects *S. cerevisiae* from oxidative stress

The substrates identified from the biotin pull down experiments and the fact that Sec-containing proteins are typically involved in redox homeostasis, led us to hypothesize that SelO is involved in the cellular response to oxidative stress. Yeast grown on non-fermentable carbon sources induce oxidative stress through mitochondrial respiration (Farrugia and Balzan, 2012; Grant et al., 1997). We detected an increase in *S. cerevisiae* SelO protein levels in cells grown on the non-fermentable carbon sources glycerol, lactate and acetate (Figure 7A). These results are consistent with previous studies showing that yeast SelO mRNA expression correlates with the stress response and is induced in respiring cells (Tu et al., 2005).

We challenged WT and SelO deficient *S. cerevisiae* with H_2O_2 and observed a decrease in survival in SelO KO cells (Figure 7B). Cell viability was fully complemented by WT SelO but not the inactive mutant. We then incubated WT and SelO KO yeast with the redox-cycling compound menadione, which increases cellular reactive oxygen species (Zadzinski et al., 1998). SelO deficient yeast displayed a menadione-dependent growth defect that was fully rescued by WT *S. cerevisiae* SelO but not the catalytically inactive mutant (Figure 7C). Collectively, these results suggest that SelO-mediated AMPylation of proteins protects *S. cerevisiae* from oxidative stress.

SelO regulates global S-glutathionylation levels in bacteria and yeast

The reversible oxidative modification of cysteine residues on proteins with a molecule of glutathione (S-glutathionylation) is emerging as a ubiquitous and essential mechanism for protecting proteins exposed to oxidative conditions (Figure S6B) (Mieyal and Chock, 2012). Under oxidative stress, protein thiols can become reversibly oxidized to sulfenic acids that are protected from over-oxidation by S-glutathionylation. Protein S-glutathionylation is reversed by the grx family of de-glutathionylation enzymes, which form a mixed disulfide intermediate to restore the free thiol on target proteins (Shelton et al., 2005). Interestingly, Tyr13 in *E. coli* grxA, which is AMPylated by SelO, lies within the highly conserved redox active site of the enzyme (^{11}C-P-Y-C^{14}) and interacts with glutathione (Figure S6C and D). Therefore, we hypothesized that SelO-mediated AMPylation of grx family members would

regulate S-glutathionylation of proteins *in vivo*. Under normal growth conditions, SelO deficient *E. coli* and yeast showed a modest decrease in global S-glutathionylation as judged by protein immunoblotting using a S-glutathionylation specific antibody (Figure 7D & E, respectively; lanes 1 and 2). However, when cells were treated with oxidized glutathione (GSSG) or diamide, conditions known to increase protein S-glutathionylation (Ghezzi et al., 2002; Sun et al., 2012), we observed a marked decrease in S-glutathionylation levels in both bacterial and yeast SelO KO cells (Figure 7D & E, respectively; lanes 4–7). Collectively, these results suggest SelO regulates protein S-glutathionylation levels by AMPylation of the grx family of enzymes.

Discussion

Our structural analysis of *P. syringae* SelO has unexpectedly discovered a previously unrecognized activity for a member of the protein kinase superfamily. There are other enzymes in nature that can AMPylate protein substrates on amino acid side chains, including glutamine synthase adenylyltransferase (GS ATase) (Shapiro and Stadtman, 1968), the Legionella effector DrrA/SidM (Muller et al., 2010) and proteins containing the Fic domain (Worby et al., 2009; Yarbrough et al., 2009). However, SelO is unique because it has a protein kinase fold. GS ATase and DrrA adopt an α+β nucleotidyltransferase fold and catalyze AMPylation using a conserved G-X_{11}-D-X-D motif (Holm and Sander, 1995). In DrrA, the second Asp of the motif acts as a general base to deprotonate the protein substrate Tyr, which then acts as a nucleophile on the α-phosphate of ATP (Gavriljuk et al., 2014). Fic family proteins adopt a mainly α-helical bundle fold with a conserved H-X-F-X-(D/E)-(A/G)-N-(G/K)-R motif (Kinch et al., 2009; Xiao et al., 2010). The Fic motif His residue acts as the general base in catalysis, while the Arg positions the β-phosphate and stabilizes the developing negative charge on the α-phosphate during catalysis (Luong et al., 2010). A second Arg just upstream of the Fic motif forms a hydrogen bond with the γ-phosphate of the bound nucleotide. Interestingly, the Fic-related Doc toxin is thought to use inverted ATP to phosphorylate protein substrates (Castro-Roa et al., 2013). Analogous to the Fic/Doc proteins, our results suggest that a flip of the ATP in protein kinases allows the switch between AMPylation and phosphorylation of protein substrates.

In each of the known folds capable of catalyzing AMPylation, a key conserved residue acts as a general base to deprotonate the protein target Tyr/Thr residue. Sequence conservation of the SelO active site suggests the catalytic Asp that performs this function (D252 in *P. syringae* SelO) has migrated from the canonical position in traditional protein kinases. Accordingly, mutagenesis supports a critical role for this residue in catalysis (Figure 4B). To gain understanding of the potential SelO peptide binding site, we superimposed the SelO kinase domain with activated FGFR2 kinase bound to a peptide substrate (Figure S7A) (Chen et al., 2007). The canonical protein kinase active site Asp (PKA; D166) approaches the substrate Tyr OH from one side, while the migrated SelO active site Asp approaches from the opposite side. A Pro residue at the C-terminus of the FGFR2 activation loop that positions the substrate peptide Tyr is replaced by a conserved aromatic residue (F82) from the SelO Gly-rich loop insert. Two additional SelO family conserved residues from the Gly-rich loop insert (Q81) and the β8-αC insert (R122) that define the flipped ATP site, might also contribute to an extended SelO peptide substrate binding site.

The SelO C-terminal domains (CTDs) bridge the regulatory αC helix with the activation loop and position the αC helix in the active conformation. This interaction resembles the activation of cyclin dependent kinase CDK2 by cyclin A (Jeffrey et al., 1995). The CDK2 regulatory αC helix PSTAIRE motif retains a conserved RE (PKA E91) in the same position as the invariant RE from SelO (Figure S7B & C). The Arg residues from both kinases form key hydrogen bond interactions with the activation loops, while the Glu residues form an ion pair with their corresponding Lys (PKA K72) marking the activated state of the protein kinase. In the absence of cyclin, the αC helix and the activation loop of free CDK2 adopt alternate conformations rendering the kinase inactive. The free CDK2 regulatory helix rotates away from the active site pocket, disrupting residues involved in orienting phosphate and coordinating Mg^{2+}. The free CDK2 activation loop covers the active site and prevents ATP access. The SelO CTD2 prevents such a rotation of the regulatory αC helix in the present SelO structure. The disordered C-terminus extending from CTD2 plays a role in inactivating the kinase by forming a disulfide bond with a Cys in the activation loop. Analogous to CDK2, this inactivation could involve a conformational change of the CTD to allow rotation of the regulatory αC helix or an alternate conformation of the activation loop driven by disulfide bond formation, or both.

Interestingly, in the crystal structure of *P. syringae* SelO, the conserved activation loop cysteine (C279, corresponding to C272 of *E. coli* SelO) is in a position compatible with formation of a disulfide bond with another cysteine, C246 (the Cβ-Cβ distance is 3.8Å). The C246 (not present in *E. coli* SelO) is located only seven residues away from the predicted catalytic D252. Thus, the activating mechanism of intramolecular disulfide exchange may be more complex in some members of the SelO family possessing more than one cysteine in the activation loop or in the catalytic loop. Future work will be needed to confirm the physiological importance of the selenylsulfide/disulfide bond and its role in regulating AMPylation activity of SelO from different species.

We have developed a strategy using a biotinylated ATP derivative to identify SelO substrates. Notably, we identified the glutaredoxins and the E1 component of the alpha ketoglutarate dehydrogenase complex, sucA, to be direct substrates of *E. coli* SelO. SucA is a component of the 2-oxoglutarate dehydrogenase complex, which catalyzes a rate-limiting step of the tricarboxylic acid cycle (TCA) and is thought to be a mitochondrial redox sensor (McLain et al., 2011). Glutaredoxin is a small redox protein involved in reducing cellular disulfides and removes glutathione from Cys residues on proteins (Shelton et al., 2005). Interestingly, grxA is AMPylated on a highly conserved active site residue suggesting that AMPylation may regulate its activity (Figure S6C & D). Indeed, total protein S-glutathionylation levels were decreased in SelO deficient *E. coli* and yeast (Figure 7D), suggesting that AMPylation of the grx family of enzymes is an evolutionarily conserved mechanism to regulate protein S-gluathionlyation levels in cells.

Tyr13 on grxA is located adjacent to the glutathione binding cysteine residue (Figure S6D) and studies have indicated that the aromatic sidechain of Tyr13 provides a niche for glutathione binding and subsequent deglutathionyation acitivity (Saaranen et al., 2009). Therefore, AMPylation of Tyr13 may impose steric hinderance for glutathione binding and would inhibit the enzyme. Similar to SelO mutants, yeast glutaredoxin mutants are more

sensitive to oxidative stress induced by menadione and hydrogen peroxide treatment (Luikenhuis et al., 1998). In the case of sucA, Thr405 lies within a disordered loop in the dimerization interface (Figure S6E & F). The loop is connected to the active site that coordinates Mg^{2+} (Frank et al., 2007; Wagner et al., 2011). Studies are underway to determine whether AMPylation of sucA regulates the formation of the alpha-ketoglutarate dehydrogenase complex and/or affects its activity. Collectively, the highly conserved SelO sequence, AMPylation sites in substrates (grxA, sucA), and enzymatic activity, suggest that SelO regulates an ancient, conserved oxidative stress defense mechanism in prokaryotes and eukaryotes.

In higher eukaryotes, SelO homologs contain a Sec, whereas a Cys is present in the equivalent position in lower eukaryotes and all prokaryotes with a SelO homolog. Most human selenoproteins have homologs in lower organisms with a Cys in place of the Sec. Incorporation of Sec is energetically expensive; however, the evolutionary advantage of using Sec as opposed to Cys is incompletely understood. Although selenoproteins are considered superior catalysts, it was recently shown that the selenoprotein glutathione peroxidase 4 (GPX4), requires its Sec to prevent irreversible over-oxidation (Ingold et al., 2018). We propose that SelO has evolved a Sec to increase the redox potential of the resulting selenylsulfide bond and/or prevent irreversible over-oxidation, both of which would regulate AMPylation activity.

In summary, we have discovered a new activity for a member of the protein kinase superfamily, which has revealed the molecular function of one of the twenty-five selenoproteins in humans. Our results highlight the structural and biochemical diversity of the protein kinase superfamily and underscore a novel mechanism of redox regulation. Importantly, our results suggest that AMPylation may be more widespread than previously appreciated and that “inactive” kinases should be analyzed for alternative transferase activities.

STAR Methods Text

CONTACT FOR REAGENT AND RESOURCE SHARING

Further information and requests for resources and reagents should be directed to and will be fulfilled by the Lead Contact, Vincent S. Tagliabracci (vincent.tagliabracci@utsouthwestern.edu)

EXPERIMENTAL MODEL AND SUBJECT DETAILS

DH5α chemically competent cells were used for molecular cloning. Rosetta (DE3) chemically Competent cells were used for protein expression and glutathionlyation assays. Both of them were grown in LB medium cultured at 37°C. After induction, Rosetta (DE3) cells were transferred to room temperature. S. cerevisiae (BY4741 and MR6) were grown in YPD or YPAD.

The following strains used in this study—Parental BY4741[*Mata leu2Δ0 met15Δ0 ura3Δ0 his3Δ1*] strain was obtained from Dharmacon and used to generate the following strains: BY4741pRS313 [*Mata leu2Δ0 met15Δ0 ura3Δ0 his3Δ2* (pRS313- HIS3/CEN-ARS/

Amp)], BY4741 ΔSelO[*Mata leu2Δ0 met15Δ0 ura3Δ0 his3Δ1 fmp40Δ::KanMX*], BY4741 ΔSelO pRS313 [*Mata leu2Δ0 met15Δ0 ura3Δ0 his3Δ1 fmp40Δ::KanMX* (pRS313- HIS3/CEN-ARS/Amp)], BY4741 ΔSelO pRS313 SelO [*Mata leu2Δ0 met15Δ0 ura3Δ0 his3Δ1 fmp40Δ::KanMX* (pRS313- WT FMP40/HIS3/CEN-ARS/Amp)], BY4741 ΔSelO pRS313 D348A SelO[*Mata leu2Δ0 met15Δ0 ura3Δ0 his3Δ1 fmp40Δ::KanMX* (pRS313- D348A FMP40/HIS3/CEN-ARS/Amp)], BY4741 cit1 mCherry pDGFP SelO[*Mata leu2Δ0 met15Δ0 ura3Δ0 his3Δ2 cit1-mCherry-HygMX* (pDGFP-P_{GAL1}-*FMP40-GFP/CEN-ARS/Amp)*], BY4741 cit1 mCherry pDGFP SelO 24-C[*Mata leu2Δ0 met15Δ0 ura3Δ0 his3Δ2 cit1-mCherry-HygMX* (pDGFP-P_{GAL1}-*FMP40 24-C-GFP/CEN-ARS/Amp)*].

Parental MR6 [*Mata ade2–1 his3–11,15 trp1–1 leu2–3,112 ura3–1 CAN1 arg8::hisG*] strain was obtained from Dr. Jean-Paul di Rago and used to generate the following strains: MR6 pRS315[*Mata ade2–1 his3–11,15 trp1–1 leu2–3,112 ura3–1 CAN1 arg8::hisG* (pRS315-LEU2/CEN-ARS/Amp)], MR6 ΔSelO[*Mata ade2–1 his3–11,15 trp1–1 leu2–3,112 ura3–1 CAN1 arg8::hisG fmp40Δ::KanMX*], MR6 ΔSelO pRS315[*Mata ade2–1 his3–11,15 trp1–1 leu2–3,112 ura3–1 CAN1 arg8::hisG fmp40Δ::KanMX* (pRS315-LEU2/CEN-ARS/Amp)], MR6 ΔSelO pRS315-WT FMP40[*Mata ade2–1 his3–11,15 trp1–1 leu2–3,112 ura3–1 CAN1 arg8::hisG fmp40Δ::KanMX* (pRS315- WT FMP40/LEU2/CEN-ARS/Amp)], MR6 ΔSelO pRS315-D348A FMP40[*Mata ade2–1 his3–11,15 trp1–1 leu2–3,112 ura3–1 CAN1 arg8::hisG fmp40Δ::KanMX* (pRS315- D348A FMP40/LEU2/CEN-ARS/Amp)].

All yeast strains were grown at 30°C in the appropriate experimental growth medium as described in the methods section.

METHOD DETAILS

Reagents—Myelin basic protein (M1891–5MG), Menadione (M5625) and AMP-PNP (A2647) were purchased from Sigma. Selenomethionine containing medium was purchased from Molecular Dimensions (MD12–500). Tris(2-carboxyethyl)phosphine hydrochloride (TCEP; 20490) and 4-acetamido-4’-maleimidylstilbene-2,2’- disulfonic acid (AMS; A485) were purchased from Thermo Fisher. Biotin-17-ATP was purchased from Enzo life sciences (ENZ-42817). High sensitivity streptavidin HRP (21130) and high capacity streptavidin agarose resin (20357) were purchased from Pierce. Rabbit anti-GroEl antibodies were purchased from Enzo life sciences (ADI-SPS-875-D). Rabbit anti-Vma6 antibodies were a generous gift from Dr. Vincent Starai (University of Georgia, Athens). Mouse anti-porin antibodies were from Invitrogen (459500), and rabbit anti-histone H3 antibodies were from Millipore (06–755). Rabbit anti-Mia40 antibodies were a generous gift from Dr. Carla Koehler (UCLA). Rabbit anti AMP-Threonine antibodies were as described previously (Hao et al., 2011). Mouse ant-GSH and anti-GAPDH antibodies were from Thermo.

Generation of constructs and strains—The *E. coli* SelO (ydiU), grxA, sucA, trxA and trxB coding sequence were amplified by PCR using Rosetta genomic DNA as a template. The *Pseudomonas syringae* SelO coding sequence was amplified by PCR using *P. syringae* DC3000 genomic DNA. The *S. cerevisiae* coding sequence was amplified using BY4741 genomic DNA as a template. *Homo sapiens* SelO cDNA clone was a generous gift from Carolyn Worby (UCSD). The amplified open reading frames were cloned into a

modified pet28a bacterial expression vector (ppSumo), containing an N-terminal 6X-His tag followed by the yeast Sumo (smt3) coding sequence or pProEX2 containing an N-terminal 6X-His tag followed by a TEV protease cleavage site.

BY4741 cit1-mCherry was derived from BY4741 (*MATa his3Δ1 leu2Δ0 met15Δ0 ura3Δ0*) using a PCR-based modification (Longtine et al., 1998). Briefly, a mCherry and hygromycin resistance cassette with homologous sequences flanking the C-terminus of the Cit1 gene was amplified by PCR. The product of the reaction was then introduced to BY4741 via a lithium acetate mediated transformation and recovered overnight in 2 mL of YPD. Recombinants were selected by plating 100 μL of the transformation on YPD agarose plates supplemented with 200 μg/mL hygromycin. Successful recombination was verified by colony PCR using primers flanking the endogenous locus and the inserted cassette.

The *S. cerevisiae* SelO (*fmp40)* gene was replaced by *KANMX4* deletion cassette in the W303–1B strain background (MR6, *MATa ade2–1 his3–11,15 trp1–1 leu2–3,112 ura3–1 CAN1 arg8::hisG*) (Rak et al., 2007). The cassette was amplified by PCR with primers FWD:5`-CGGTGATATGAGGTGATCGTGG-3` and REV:5`-GGTGCCAGTCGTTCGG-3`, using total gDNA isolated from *fmp40::KANMX4* deletion mutant as a template (Euroscarf collection). After transformation and selection on plates supplemented with geneticin at 200 μg/ml. Deletions were verified by PCR using primers 5`-GAACTCCGGAATTGGACGATG-3` and internal primer to the KANMX4 gene 5'-GGATGTATGGGCTAAATGTACG-3'.

For yeast complementation experiments, the *S. cerevisiae* SelO gene containing 1000 bp upstream of the ATG and 500 bp of the 3'UTR was cloned into the pRS313 vector using Not1 and Spe1 endonucleases. The FMP40 gene was then subcloned into the pRS315 vector using Not1 and Sma1, which deleted ~130 bp from the 3'UTR.

The *E. coli* SelO (ydiU) gene was disrupted using the λ red recombinase-mediated recombination system (Datsenko and Wanner, 2000). Briefly, a tetracycline resistance cassette flanked with 50 bp homologous to the ydiU gene was amplified via PCR. The reaction product was electroporated into the Rosetta *E. coli* strain carrying the λ red recombinase plasmid pKD46 (a generous gift from the Dr. Vanessa Sperandio). Transformants were selected by growth on LB agar plates containing tetracycline (10 μg/ml) and simultaneously cured of pKD46 by growth at 37°C overnight. Disruption of the *ydiU* gene was confirmed by colony PCR, using primers flanking the endogenous locus and the inserted cassette.

Protein purification—*E. coli, P. syringae, S. cerevisiae* or *H. sapiens* SelO, cloned into ppSumo, were transformed into Rosetta DE3 cells. Cells were grown in Luria Bertani (LB) broth to OD_{600} of 0.6–0.8. Protein expression was induced with 0.4 mM IPTG for 16–18 hours at room temperature. Cells were harvested by centrifugation and lysed in 50mM Tris-HCl pH 8, 300 mM NaCl, 1 mM PMSF by sonication. Cell lysates were cleared by centrifugation at 25,000 −30,000 × g for 25–30 minutes. The cleared lysate was incubated with washed Ni-NTA beads for one hour at 4°C. Beads were passed over a column and washed with 20 column volumes of 50 mM Tris-HCl pH 8, 300 mM NaCl, 10–25 mM

imidazole. Fusion proteins were eluted with 50mM Tris-HCl pH 8, 300 mM NaCl, 300 mM imidazole. Proteins were cut overnight at 4°C with 6X-His tagged ULP Sumo protease followed by gel filtration chromatography using a Superdex 200 gel filtration column attached to an AKTA Pure FPLC chromatography system (GE Healthcare). When proteins were purified in the presence of reducing agent, 0.1% β-mercaptoethanol was added to the lysis buffer. The wash, elution and gel filtration buffers contained 1 mM DTT.

In vitro AMPylation assays—For comparison of [$\gamma-^{32}$P]ATP with [$\alpha-^{32}$P]ATP, assays were performed using purified, untagged *E. coli, S. cerevisiae* or *H. sapiens* SelO in a reaction mixture containing 50 mM Tris-HCl pH 8, 5 mM $MgCl_2$, 100 μM [$\gamma-^{32}$P]ATP or [$\alpha-^{32}$P]ATP (specific radioactivity = 3000 cpm/pmol), 5mM DTT, and 100 μg/mL SelO proteins. Reactions were incubated at 37°C for 30 minutes and terminated by adding 25 mM EDTA. SDS loading buffer was then added to the samples and boiled. Reaction products were resolved by SDS-PAGE and stained with Coomassie blue.

Typically, AMPylation assays were performed in a reaction mixture containing 50 mM Tris-HCl pH 8, 5 mM $MgCl_2$, 100 μM [$\alpha-^{32}$P]ATP (SA = 500–3000 cpm/pmol), 10–50 μg/mL SelO, and 250 μg/mL of substrate (myelin basic protein or grxA). Reactions were also performed with 5 mM DTT, 0.1mM to 2mM excess GTP, CTP or UTP nucleotide, or with the thioredoxin system (13 μM *E. coli* trxA, 5 μM *E. coli* trxB and 200 μM NADPH). Reactions were incubated at 37°C for various time points and terminated by adding EDTA. SDS loading buffer containing 1% β-mercaptoethanol was added to samples and boiled. Samples were resolved by SDS-PAGE and stained with Coomassie blue.

For SelO point mutant AMPylation reactions (Figure 4B), assays were performed using Sumo tagged *E. coli* SelO, under the same conditions as above for 15 min using 250 μg/mL MBP as substrate. Reactions were terminated by adding EDTA and SDS loading buffer with 1% β-mercaptoethanol and boiled. Reaction products were resolved by SDS-PAGE and stained with Coomassie blue. MBP bands were excised and the incorporated radioactivity was quantified by scintillation counting using a Beckman scintillation counter.

For non-radioactive auto AMPylation reactions, untagged *E. coli or* human SelO was incubated in 50 mM Tris-HCl pH8, 5 mM $MgCl_2$, 100 μM ATP, 5mM DTT for 1 hour at 37°C. Reactions were terminated by adding EDTA and SDS loading buffer with 1% β-mercaptoethanol and boiled. Reaction products were resolved by SDS-PAGE, transferred to nitrocellulose membrane and immunoblotted with rabbit anti-Thr AMP antibody. Immunoblotting was essentially performed as described (Tagliabracci et al., 2015). Briefly, membranes were blocked with 5% BSA for 1 hour at room temperature. The membranes were briefy rinsed with filtered 50 mM Tris-HCl pH = 7.5, 150 mM NaCl, 0.1% tween 20 (TBST). Membranes were incubated with anti-Thr AMP antibody (1:1000) diluted in 2% nonfat dry milk (Kroger) overnight at 4°C with shaking. The membranes were washed 3–4X for 10 min each with TBST at room temperature. The membranes were then probed with donkey anti-rabbit IgG, HRP linked (1:5000 in 2% milk) for 1 hour at room temperature followed by 3–4 washes with TBST and detection by chemiluminescence.

SelO reduction assay—For redox assays, 100 μg/mL (1.8 μM) untagged *E. coli* SelO was incubated with 0, 0.03, 0.1, 0.3 or 1 mM DTT in 50 mM Tris-HCl pH 7.5, 150 mM NaCl for 1 hour at room temperature. SDS loading buffer without reducing agent was added to samples and boiled. Samples were resolved by SDS-PAGE and stained with Coomassie blue.

Production of *S. cerevisiae* SelO antibodies—*S. cerevisiae* SelO was purified as a 6X His Sumo fusion protein as above and the His-Sumo tag was cleaved with ULP1. The untagged protein was purified by Superdex 200 gel filtration chromatography and used to inoculate rabbits for generation of rabbit anti-*S. cerevisiae* SelO anti-serum (Cocalico Biologicals). Total IgG was partially purified by ammonium sulfate precipitation (Kent, 1999) then passed over a HiTrap NHS-activated HP column (GE Healthcare) linked to 6X His Sumo to remove any potential contaminating anti-Sumo IgG. Anti-*S. cerevisiae* SelO antibodies were affinity-purified from the flow through by coupling *S. cerevisiae* SelO to a new HiTrap NHS-activated HP column essentially as described (Wollweber, 1990).

***S. cerevisiae* confocal microscopy—**The *S. cerevisiae* SelO (*fmp40*) was cloned into a modified yeast expression vector containing a C-terminal GFP-myc tag (pDGFP) (Salomon et al., 2013). The BY4741 cit1 mCherry strain was transformed with empty vector, pDGFP, pDGFP *S. cerevisiae* SelO or pDGFP *S. cerevisiae* SelO 24-C. Transformed cells were grown overnight in synthetic drop-out (SD) medium without uracil and containing 2% glucose. The following day, cells were harvested by centrifugation and washed three times with sterile water. Cells were placed in culture at 30°C with shaking for 8 hours in SD-medium without uracil and containing 1% Galactose / 2% Raffinose. Cells were spotted on glass coverslip and used for confocal imaging on a Zeiss LSM 800 confocal microscope.

***S. cerevisiae* mitochondria isolation—**Yeast mitochondria were isolated as previously described (Gregg et al., 2009). Briefly, yeast cells were pelleted by centrifugation at 3000 × g for 5 min and the cells were washed with water then resuspended in DTT buffer (100 mM Tris-HCl pH 9.4, 10mM DTT). The cells were then incubated with shaking at 30°C for 20 min and pelleted by centrifugation. Cells were washed with zymolase buffer (20 mM potassium phosphate pH = 7.4, 1.2 M sorbitol) and resuspended in zymolase buffer containing lyticase. Cells were incubated at 30°C for 30 min with shaking, then pelleted by centrifugation at 2200 × g for 5 min at 4°C. The resulting spheroplasts were washed with ice cold homogenization buffer (10 mM Tris-HCl pH = 7.4, 0.6 M sorbitol, 1 mM EDTA, 0.2% BSA). Spheroplasts were resuspended in ice cold homogenization buffer and lysed using a glass dounce homogenizer. Spheroplasts were then centrifuged at 1500 × g for 5 min at 4°C and the supernatant was centrifuged at 3000 × g for 5 min at 4°C. The resulting supernatant was further centrifuged at 12,000 × g for 15 min at 4°C. The pellet was resuspended in SEM buffer (10 mM MOPS KOH pH = 7.2, 250 mM sucrose, 1 mM EDTA) and centrifuged at 3000 × g for 5 min at 4°C. The supernatant was centrifuged at 12,000 × g for 15 min at 4°C. The pellet, which contains enriched mitochondria, was used for SelO TCA precipitation and glutathionylation assays (see below).

***S. cerevisiae* sucrose gradient fractionation—**BY4741 or BY4741 Δ*SelO* (Dharmacon YSC1053) were grown overnight at 30°C in YPD broth (20 g/L peptone, 10 g/L yeast extract, 2% glucose) and harvested by centrifugation. Yeast cells were disrupted and fractionated as described above. The enriched mitochondrial pellet was applied to a sucrose gradient, which was prepared by overlaying 15% sucrose in EM buffer (10 mM MOPS KOH pH = 7.2, 1 mM EDTA) over 30%, 45%, 60% and 75% sucrose. Proteins (2 μg) from each sucrose gradient fraction were resolved by SDS-PAGE, transferred to nitrocellulose and immunoblotted with rabbit anti-*S. cerevisiae* SelO, mouse anti-porin, rabbit anti-Vma6 or rabbit anti-histone H3 antibodies.

SelO TCA precipitation—BY4741 or BY4741 Δ*SelO* grown in YPD broth overnight at 30°C was harvested by centrifugation. Yeast mitochondria were isolated as described above. Mitochondria (100 μg) were pelleted and resuspended in 1 mL of 10% ice cold trichloroacetic acid (TCA). Mitochondrial proteins were precipitated on ice for 1 hour, then centrifuged at 20,000 × g for 10 minutes at 4°C. Precipitated pellets were washed with 1 mL of ice cold acetone and centrifuged at 20,000 × g for 5 minutes at 4°C. Pellets were air dried and resuspended in 200 μL of 500 mM Tris-HCl, pH 7.5, 2% SDS and 1 mM EDTA. Samples were incubated for 10 minutes at room temperature in the presence or absence of 5 mM DTT. SDS loading buffer without reducing agent was added to the samples, which were subsequently resolved by SDS-PAGE and transferred to nitrocellulose membrane.

SelO cysteine mutant reduction assay—*E. coli* SelO was purified as described above in the absence of reducing agent. Untagged *E. coli* SelO (100 μg/mL) was incubated in the presence or absence of 1 mM TCEP and/or 5 mM AMS for 2 hours at room temperature in the dark. SDS loading buffer without reducing agent was added to samples. Samples were resolved by SDS-PAGE and stained with Coomassie blue.

Biotin-17-ATP AMPylation assay—Assays were performed using purified untagged *E. coli* SelO in a reaction mixture containing 50 mM Tris-HCl pH 8, 5 mM $MgCl_2$, 5mM DTT, 500 μM biotin-17-ATP, 200 μg/mL SelO, 300 μg/mL *E. coli* cell lysate or yeast mitochondrial extracts. Reactions were also performed after pretreating *E. coli* and yeast mitochondria with either 2 mM H_2O_2 (*E. coli*) or 0.5 mM (yeast mitochondria). Biotinylation reactions were incubated at 37°C for 30 minutes and terminated by the addition of EDTA and SDS loading buffer with 1% β-mercaptoethanol and boiled. Reaction products were resolved by SDS-PAGE and transferred to nitrocellulose membranes. The Streptavidin HRP blot was performed as previously described (Roux et al., 2013). Briefly, the membranes were incubated in 1X PBS containing 1% BSA and 0.2% Triton X-100 for 30 min at room temperature. The membranes were then incubated with strepdavidin-HRP at 1:40,000 dilution in 1X PBS containing 1% BSA and 0.2% Triton X-100 with shaking overnight at 4°C. Membranes were washed and blocked with 1X PBS containing 10% adult bovine serum and 1% Triton X-100 for 5 min at room temperature. Membranes were washed with 1X PBS and blots were developed using ECl and visualized by chemiluminescence For streptavidin agarose pulldowns, reactions were terminated with EDTA, then affinity purified using streptavidin agarose as previously described (Roux et al., 2013). Briefly, the streptavidin agarose beads containing the biotinylated proteins were washed with 2% SDS

for 8 min at room temperature followed by washing with 50 mM HEPES pH = 7.5, containing 0.1% deoxycholic acid, 1% Triton X-100, 1 mM EDTA and 500mM NaCl. The beads were then washed again with 10mM Tris-HCl pH = 7.4, 0.5% deoxycholic acid, 0.5% NP-40, 1 mM EDTA and 250 mM LiCl followed by a final wash with 50mM Tris-HCl pH = 7.4 prior to MS analysis.

In vivo sucA and grxA AMPylation assays—*E. coli* sucA and grxA were cloned into the MCS1 of petDuet1 in frame with an N-terminal 6X His tag. *E. coli* SelO was cloned without a tag into the MCS2 of petDuet1. SelO D256A, sucA T405A and sucA S404A were generated by site directed mutagenesis as described (Nguyen et al., 2016). Briefly, primers were designed using the Agilent Quick Change Primer design tool: https://www.genomics.agilent.com/primerDesignProgram.jsp and used in PCR reaction to generate the desired mutation using PfuTurbo DNA polymerase (Thermo). Reaction products were digested with Dpn1 restriction endonuclease and mutations were confirmed by sequencing plasmids. petDuet-sucA:SelO or petDuet-grxA:SelO (or mutants) were transformed into Rosetta DE3 Δ *E. coli* SelO (ydiU) strain. Cells were grown in LB broth to OD_{600} = 0.6–0.8. Protein expression was induced by the addition of 0.4 mM IPTG overnight at room temperature and the His tagged proteins were purified as described above in the presence of reducing agent. His tagged proteins were further purified by Superdex 200 gel filtration column using AKTA Pure FPLC chromatography system. SucA (2 μg) was resolved by SDS-PAGE and immunoblotted with rabbit anti-Thr AMP antibody. sucA and grxA (5 μg) were resolved by SDS PAGE in preparation for mass spectrometry.

Hydrogen peroxide viability assays—The MR6 strain was transformed with the empty pRS315 vector. The MR6 Δ *S. cerevisiae* SelO strain was transformed with empty vector, WT *S. cerevisiae* pRS315-SelO or pRS315- *S. cerevisiae* SelO D348A. Exponential growth-phase cultures (OD=1) in glucose minimal medium (0.67% Yeast Nitrogen Base, 2% glucose, leucine Drop-out amino acids, adenine 40 mg/L) were treated with 0.1 mM H_2O_2 for 200 minutes with shaking at 28°C. The cell survival in the culture at time zero (before the hydrogen peroxide treatment) and after were estimated by plating the cells on the YPD-adenine plates (1% Yeast Extract, 1 % bacto peptone, 2 % glucose, 2% Bacto agar, adenine 40 mg/L). The % survival was normalized to the number of cells at time zero. Results are representative of three independent experiments.

Menadione viability assays—BY4741 was transformed with empty pRS313 vector. BY4741 Δ *S. cerevisiae* SelO strain was transformed with empty vector, WT *S. cerevisiae* pRS313-SelO or pRS313- *S. cerevisiae* SelO D348A. Exponential growth phase cultures in glucose synthetic drop-out medium without histidine (6.7 g/L yeast nitrogen base without amino acids, 1.4 g/L yeast synthetic drop-out medium supplement and containing 2% [w/v] glucose and leucine, tryptophan, uracil; (Salomon and Sessa, 2010), were treated with 0.6 mM menadione for 1 hour at 30°C. Post treatment, cells were serial diluted ten-fold and spotted on synthetic drop-out plates. Cells were grown for 2–3 days prior to imaging.

Mass spectrometry analysis—Sample preparation included the excision of proteins from polyacrylamide gels that were separated by SDS-PAGE and stained with Coomassie

blue. Protein gel samples were reduced and alkylated using DTT and iodoacetamide, respectively. Note, reduction and alkylation of cysteine residues was not performed on the sample containing unreduced *E. coli* SelO peptides linked by the disulfide bond (Figure 5). Enzymatic overnight digestion (37°C) was performed on all samples using trypsin and samples were de-salted using solid phase extraction (SPE) prior to mass spectrometry analysis. LC-MS/MS experiments were performed on a Thermo Scientific EASY-nLC 1200 liquid chromatography system coupled to a Thermo Scientific Orbitrap Fusion Lumos mass spectrometer. To generate MS/MS spectra, MS1 spectra were first acquired in the Orbitrap mass analyzer with a resolution of 120,000. Peptide precursor ions were isolated and fragmented using high-energy collision-induced dissociation (HCD). The resulting MS/MS fragmentation spectra were acquired in the ion trap. MS/MS spectral data was then searched using the Mascot search engine (Matrix Science) for peptide identification. Carbamidomethylation of cysteine residues (+57.021 Da) was set as a static modification for searches, while oxidation of methionine (+15.995 Da) and AMPylation of serine/tyrosine/threonine (+329.053 Da) were set as dynamic modifications. The precursor ion tolerance was set to 15 ppm and the product ion tolerance was set to 0.6 Da for all searches. The MS/MS spectrum of the *E. coli* SelO peptides linked by the disulfide bond were first identified using Thermo BioPharma Finder software and confirmed via manual verification and assignment of fragment ions. Carbamidomethylation of cysteine residues was not included as a modification for this search, as the sample was not reduced/alkylated. Additionally, the identification of all AMPylated peptides were manually verified from the MS/MS spectra of the modified peptides and their unmodified counterparts. Unique ions (136.1, 250.1, and 348.1 Da) corresponding to the neutral loss of the AMP group from peptides during HCD were present in the MS/MS spectra of AMPylated peptides.

Analysis of S. cerevisiae SelO expression—MR6 and MR6 ΔSelO strain was grown in YPAD overnight, then diluted into YP medium with either 2% glucose, 2% galactose, 2% raffinose, 3% glycerol, 2% potassium acetate, or 2% sodium lactate. Cells were harvested following overnight incubation at 30°C and extracts were prepared as described previously (Salomon and Sessa, 2010). Briefly, 1OD of yeast cells were centrifuged at 800 × g for 5 min at room temperature. Cells were resuspended in 100uL of ice cold yeast lysis buffer (200 mM NaOH and 0.5% β-mercaptoethanol) and incubated on ice for 30 min. The pH of the lysate was adjusted to ~7 by the addition of 6M HCl. SDS loading buffer containing 1% β-mercaptoethanol was added and the samples were boiled prior to SDS PAGE.

***E. coli* protein S-glutathionylation experiments—**Rosetta and Rosetta Δ SelO strains were transformed with empty pBad MycHis vector. Cultures were grown in M9 minimal medium with ampicillin for 48 hours. Cells (1 OD) were resupended in 1xPBS and treated with 1 mM GSSG or 1 mM diamide for 25 minutes at room temperature. Post treatment, 10 mM NEM was added to the cells and incubated for 5 minutes at room temperature. SDS loading buffer without reducing agent was added to the samples, which were subsequently resolved by SDS-PAGE, transferred to nitrocellulose membranes and analyzed for protein S-glutathionylation using the anti-GSH antibody (Virogen/Thermo) and GroEL.

Yeast protein S-glutathionylation experiments—MR6 and MR6 Δ *S. cerevisiae* SelO strains were grown in YP-glycerol to OD of 0.9. Mitochondria were isolated as described above and treated with 0.5 mM GSSG and/or 0.1 mM diamide for 30 minutes at room temperature. Post treatment, 10 mM NEM was added to the cells and incubated for 5 minutes at room temperature. SDS loading buffer without reducing agent was added to the samples, which were subsequently resolved by SDS-PAGE, transferred to nitrocellulose membranes and analyzed for protein S-glutathionylation using the anti-GSH antibody (Virogen/Thermo) and porin.

Crystallization and structure determination—*P. syringae* SelO at 10 mg/mL in 17 mM Tris-HCl pH 8, 100 mM NaCl, 1mM TCEP, 5 mM $MgCl_2$, 1 mM AMP-PNP was crystallized at 20˚C using the sitting drop vapor-diffusion method with a reservoir solution containing 200 mM calcium acetate, and 22% (w/v) PEG 3350. The crystals were cryo-protected with 200 mM calcium acetate, 22% (w/v) PEG 3350, 100 mM NaCl and 30% ethylene glycol and then flash-cooled in liquid nitrogen. Native crystals diffracted to a minimum Bragg spacing (d_{min}) of 2.27 Å and exhibited the symmetry of space group I222 with cell dimensions of a = 136.2 Å, b = 158.1 Å, c = 227.3 Å and contained four SelO molecules per asymmetric unit. All diffraction data were collected at beamline 19-ID (SBC-CAT) at the Advanced Photon Source (Argonne National Laboratory, Argonne, Illinois, USA) and processed in the program *HKL-3000* (Minor et al., 2006) with applied corrections for effects resulting from absorption in a crystal and for radiation damage (Borek et al., 2003; Otwinowski et al., 2003), the calculation of an optimal error model, and corrections to compensate the phasing signal for a radiation-induced increase of non-isomorphism within the crystal (Borek et al., 2010; Borek et al., 2013). These corrections were crucial for successful phasing. Phases were obtained from a single wavelength anomalous dispersion (SAD) experiment using the selenomethionyl-derivatized SelO protein with data to 2.2 Å. Forty-seven selenium sites were located, phases improved and an initial model containing 98% of all SelO residues was automatically generated in the *AutoBuild* routine of the *Phenix* program suite (Adams et al., 2010). Completion of this model was performed by manual rebuilding in the program *Coot* (Emsley et al., 2010). Positional and isotropic atomic displacement parameter (ADP) as well as TLS ADP refinement was performed to a resolution of 2.27 Å for the Mg^{2+}-Ca^{2+}-AMP-PNP-bound SelO using the program *Phenix* with a random 1.8% of all data set aside for an R_{free} calculation. The final model for SelO (R_{work} = 18.8%, R_{free} = 21.2%) contained 1,902 residues, four molecules of Mg^{2+}-Ca^{2+}-AMP-PNP, ten additional Ca^{2+} ions, four Cl^{-} ions, twenty-two ethylene glycol molecules, five polyethylene glycol molecules, four acetates and 590 waters. Residue Asp262 in all four monomers are outliers in a Ramachandran plot as defined in the program *MolProbity* (Chen et al., 2010); the sidechain carboxylate of this residue coordinates the metals of the Mg^{2+}-Ca^{2+}-AMP-PNP. Data collection and structure refinement statistics are summarized in Table S1.

Comparison of SelO active site with Csk1—Structures for canonical kinases (PKs) were selected from a Dalilite (Holm et al., 2008) search against the PDB with hits having DaliZ scores above 8. The structure for IRAK-4 was one of the top-scoring hits: PDB:2nru (DaliZ 9.7) and the structure for Csk1 included a bound ATP: 1csn (DaliZ 8.6). Dalilite

alignments against the *P. syringae* structure were used to assemble the multiple sequence alignment of SelO family representatives. The Dalilite structure superposition of Csk1 and *P. syringae* SelO was viewed in Pymol (Schrodinger, 2015) to compare bound nucleotide positions, with the Mg^{2+} and α-, β- and γ -phosphates of AMP-PNP in the SelO structure superimposing with the Mg^{2+} and flipped γ -, β-, and α-phosphates, respectively.

Conservation of human kinases and selenoproteins compared to bacterial homologs—Human protein kinase domain sequences were fetched from www.kinase.com. Domains other than protein kinase-like (PKL) fold were excluded, leaving total of 516 kinase domains. This set was augmented by five human members of the FAM69 family, two members of the FAM198 family, and the SELO protein. Further, this set was augmented by PKL domains from 34 human proteins belonging to the following Pfam (Finn et al., 2016) families: APH, PI3_PI4_kinase, PI3Ka, PIP5K, Fructosamin_kin, IPK, Ins_P5_2-kin, KIND, that were not included in the kinase.com dataset.

The combined dataset included 558 human protein kinase-like (PKL) domains. The protein BLAST program was used to find, for every PKL query, the closest bacterial homolog within the collection of bacterial Reference Proteomes (rp55 list, 2601913 sequences) (Chen et al., 2011). 315 kinases had homologues in bacteria satisfying the requirement of E-value below 0.001.

In a similar fashion, the protein BLAST program was used to find for every of the 25 human selenoproteins its closest bacterial homologue. Out of the 25 selenoproteins, 17 had a bacterial homologue thus defined.

SelO family sequence logo—The sequence of SelO from *Pseudomonas syringae pv. tomato str. DC3000* was subjected to 7 iterations of Jackhmmer search (Finn et al., 2015) against Reference Proteomes in order to build a collection of homologues. The search yielded 3427 aligned protein sequences. The alignment was filtered as to retain only columns present in the *P. syringae* SelO, and used as input to the WebLogo server as shown in Figure S1 (Crooks et al., 2004).

SelO sequences were collected using BLAST (Altschul et al., 1997) (E.value cutoff 0.001) against the filtered RefSeq sequence database with the *P.syringae* sequence (PBQ12144.1) as a query. Sequences were aligned using MAFFT (Katoh and Standley, 2013) to generate conservations and representatives from *E.coli* (NP_416221.1), human (NP_113642.1), yeast (Q08968.1) and plant (NP_196807.2) were selected for the alignment in Figure 1A.

Replication—All experiments were performed 3 times unless otherwise stated.

QUANTIFICATION AND STATISTICAL ANALYSIS

Quantification of yeast cell survival following H_2O_2 treatment is represented as the mean of three independent experiments (n = 3). A student T-test was used to calculate a p value using GraphPad Prism 7. Error bars represent the standard error of the mean (SEM).

DATA AND SOFTWARE AVAILABILITY

The accession number for the coordinates and structure factors reported in this paper is PDB 6EAC.

Supplementary Material

Refer to Web version on PubMed Central for supplementary material.

Acknowledgements

We thank Drs. Joseph Goldstein, Eric Olson, Peter Roach, Greg Taylor, Amanda Casey and members of the Tagliabracci laboratory for insightful discussions. We also thank Christine Nolan and Greg Urquhart for technical assistance. Results shown in this report are derived from work performed at the Argonne National Laboratory, Structural Biology Center at the Advanced Photon Source. This work was supported by NIH Grants R00DK099254 (V.S.T.), GM094575 (N.V.G), GM115188 (K.O.), T32DK007257-37 (A.S.) and T32GM008203-29 (V.A.L.), Welch Foundation Grants I-1911 (V.S.T), I-1505 (N.V. G), I-1561 (K.O.), the Once upon a Time…Foundation (K.O.) and a CPRIT grant RP170674 (V.S.T.) and the Polish National Science Centre grant 2014/15/B/NZ1/03359 (K.P.). V.S.T. is the Michael L. Rosenberg Scholar in Medical Research and a Cancer Prevention Research Institute of Texas Scholar (RR150033).

References

Adams PD, Afonine PV, Bunkoczi G, Chen VB, Davis IW, Echols N, Headd JJ, Hung LW, Kapral GJ, Grosse-Kunstleve RW, et al. (2010). PHENIX: a comprehensive Python-based system for macromolecular structure solution. Acta Crystallogr D Biol Crystallogr 66, 213–221. [PubMed: 20124702]

Altschul SF, Gish W, Miller W, Myers EW, and Lipman DJ (1990). Basic local alignment search tool. J Mol Biol 215, 403–410. [PubMed: 2231712]

Altschul SF, Madden TL, Schaffer AA, Zhang J, Zhang Z, Miller W, and Lipman DJ (1997). Gapped BLAST and PSI-BLAST: a new generation of protein database search programs. Nucleic Acids Res 25, 3389–3402. [PubMed: 9254694]

Bailey FP, Byrne DP, McSkimming D, Kannan N, and Eyers PA (2015). 2) Going for broke: targeting the human cancer pseudokinome. Biochem J 466, 201.

Borek D, Cymborowski M, Machius M, Minor W, and Otwinowski Z (2010). Diffraction data analysis in the presence of radiation damage. Acta Crystallogr D Biol Crystallogr 66, 426–436. [PubMed: 20382996]

Borek D, Dauter Z, and Otwinowski Z (2013). Identification of patterns in diffraction intensities affected by radiation exposure. J Synchrotron Radiat 20, 37–48. [PubMed: 23254654]

Borek D, Minor W, and Otwinowski Z (2003). Measurement errors and their consequences in protein crystallography. Acta Crystallogr D Biol Crystallogr 59, 2031–2038. [PubMed: 14573959]

Byrne DP, Foulkes DM, and Eyers PA (2017). Pseudokinases: update on their functions and evaluation as new drug targets. Future Med Chem 9, 245–265. [PubMed: 28097887]

Casey AK, and Orth K (2017). Enzymes Involved in AMPylation and deAMPylation. Chem Rev.

Castro-Roa D, Garcia-Pino A, De Gieter S, van Nuland NAJ, Loris R, and Zenkin N (2013). The Fic protein Doc uses an inverted substrate to phosphorylate and inactivate EF-Tu. Nat Chem Biol 9, 811–817. [PubMed: 24141193]

Chen C, Natale DA, Finn RD, Huang H, Zhang J, Wu CH, and Mazumder R (2011). Representative proteomes: a stable, scalable and unbiased proteome set for sequence analysis and functional annotation. PLoS One 6, e18910. [PubMed: 21556138]

Chen H, Ma J, Li W, Eliseenkova AV, Xu C, Neubert TA, Miller WT, and Mohammadi M (2007). A molecular brake in the kinase hinge region regulates the activity of receptor tyrosine kinases. Mol Cell 27, 717–730. [PubMed: 17803937]

Chen VB, Arendall WB 3rd, Headd JJ, Keedy DA, Immormino RM, Kapral GJ, Murray LW, Richardson JS, and Richardson DC (2010). MolProbity: all-atom structure validation for

macromolecular crystallography. Acta Crystallogr D Biol Crystallogr 66, 12–21. [PubMed: 20057044]

Collet JF, and Messens J (2010). Structure, function, and mechanism of thioredoxin proteins. Antioxid Redox Signal 13, 1205–1216. [PubMed: 20136512]

Crooks GE, Hon G, Chandonia JM, and Brenner SE (2004). WebLogo: a sequence logo generator. Genome Res 14, 1188–1190. [PubMed: 15173120]

Cui J, Xiao J, Tagliabracci VS, Wen J, Rahdar M, and Dixon JE (2015). A secretory kinase complex regulates extracellular protein phosphorylation. eLife 4.

Datsenko KA, and Wanner BL (2000). One-step inactivation of chromosomal genes in Escherichia coli K-12 using PCR products. Proc Natl Acad Sci U S A 97, 6640–6645. [PubMed: 10829079]

Dudkiewicz M, Lenart A, and Pawlowski K (2013). A novel predicted calcium-regulated kinase family implicated in neurological disorders. PLoS One 8, e66427. [PubMed: 23840464]

Dudkiewicz M, Szczepinska T, Grynberg M, and Pawlowski K (2012). A novel protein kinase-like domain in a selenoprotein, widespread in the tree of life. PLoS One 7, e32138. [PubMed: 22359664]

Emsley P, Lohkamp B, Scott WG, and Cowtan K (2010). Features and development of Coot. Acta Crystallogr D Biol Crystallogr 66, 486–501. [PubMed: 20383002]

Eyers PA, and Murphy JM (2013). Dawn of the dead: protein pseudokinases signal new adventures in cell biology. Biochemical Society transactions 41, 969–974. [PubMed: 23863165]

Farrugia G, and Balzan R (2012). Oxidative stress and programmed cell death in yeast. Front Oncol 2, 64. [PubMed: 22737670]

Fedorov O, Muller S, and Knapp S (2010). The (un)targeted cancer kinome. Nat Chem Biol 6, 166–169. [PubMed: 20154661]

Finn RD, Clements J, Arndt W, Miller BL, Wheeler TJ, Schreiber F, Bateman A, and Eddy SR (2015). HMMER web server: 2015 update. Nucleic Acids Res 43, W30–38. [PubMed: 25943547]

Finn RD, Coggill P, Eberhardt RY, Eddy SR, Mistry J, Mitchell AL, Potter SC, Punta M, Qureshi M, Sangrador-Vegas A, et al. (2016). The Pfam protein families database: towards a more sustainable future. Nucleic Acids Res 44, D279–285. [PubMed: 26673716]

Fischer EH (2013). Cellular regulation by protein phosphorylation. Biochem Biophys Res Commun 430, 865–867. [PubMed: 23058924]

Frank RA, Price AJ, Northrop FD, Perham RN, and Luisi BF (2007). Crystal structure of the E1 component of the Escherichia coli 2-oxoglutarate dehydrogenase multienzyme complex. J Mol Biol 368, 639–651. [PubMed: 17367808]

Galperin MY, and Koonin EV (2004). 'Conserved hypothetical' proteins: prioritization of targets for experimental study. Nucleic Acids Res 32, 5452–5463. [PubMed: 15479782]

Gavriljuk K, Schartner J, Itzen A, Goody RS, Gerwert K, and Kotting C (2014). Reaction mechanism of adenylyltransferase DrrA from Legionella pneumophila elucidated by time-resolved fourier transform infrared spectroscopy. J Am Chem Soc 136, 9338–9345. [PubMed: 24950229]

Ghezzi P, Romines B, Fratelli M, Eberini I, Gianazza E, Casagrande S, Laragione T, Mengozzi M, Herzenberg LA, and Herzenberg LA (2002). Protein glutathionylation: coupling and uncoupling of glutathione to protein thiol groups in lymphocytes under oxidative stress and HIV infection. Mol Immunol 38, 773–780. [PubMed: 11841837]

Grant CM, MacIver FH, and Dawes IW (1997). Mitochondrial function is required for resistance to oxidative stress in the yeast Saccharomyces cerevisiae. FEBS Lett 410, 219–222. [PubMed: 9237633]

Gregg C, Kyryakov P, and Titorenko VI (2009). Purification of mitochondria from yeast cells. J Vis Exp.

Han SJ, Lee BC, Yim SH, Gladyshev VN, and Lee SR (2014). Characterization of mammalian selenoprotein o: a redox-active mitochondrial protein. PLoS One 9, e95518. [PubMed: 24751718]

Hao YH, Chuang T, Ball HL, Luong P, Li Y, Flores-Saaib RD, and Orth K (2011). Characterization of a rabbit polyclonal antibody against threonine-AMPylation. J Biotechnol 151, 251–254. [PubMed: 21185336]

Holm L, Kaariainen S, Rosenstrom P, and Schenkel A (2008). Searching protein structure databases with DaliLite v.3. Bioinformatics 24, 2780–2781. [PubMed: 18818215]

Holm L, and Rosenstrom P (2010). Dali server: conservation mapping in 3D. Nucleic Acids Res 38, W545–549. [PubMed: 20457744]

Holm L, and Sander C (1995). DNA polymerase beta belongs to an ancient nucleotidyltransferase superfamily. Trends Biochem Sci 20, 345–347. [PubMed: 7482698]

Ingold I, Berndt C, Schmitt S, Doll S, Poschmann G, Buday K, Roveri A, Peng X, Porto Freitas F, Seibt T, et al. (2018). Selenium Utilization by GPX4 Is Required to Prevent Hydroperoxide-Induced Ferroptosis. Cell 172, 409–422 e421. [PubMed: 29290465]

Jeffrey PD, Russo AA, Polyak K, Gibbs E, Hurwitz J, Massague J, and Pavletich NP (1995). Mechanism of CDK activation revealed by the structure of a cyclinA-CDK2 complex. Nature 376, 313–320. [PubMed: 7630397]

Jura N, Shan Y, Cao X, Shaw DE, and Kuriyan J (2009). Structural analysis of the catalytically inactive kinase domain of the human EGF receptor 3. Proc Natl Acad Sci U S A 106, 21608–21613. [PubMed: 20007378]

Katoh K, and Standley DM (2013). MAFFT multiple sequence alignment software version 7: improvements in performance and usability. Molecular biology and evolution 30, 772–780. [PubMed: 23329690]

Kent UM (1999). Purification of antibodies using ammonium sulfate fractionation or gel filtration. Methods Mol Biol 115, 11–18. [PubMed: 10098159]

Kinch LN, Yarbrough ML, Orth K, and Grishin NV (2009). Fido, a novel AMPylation domain common to fic, doc, and AvrB. PLoS One 4, e5818. [PubMed: 19503829]

Kryukov GV, Castellano S, Novoselov SV, Lobanov AV, Zehtab O, Guigo R, and Gladyshev VN (2003). Characterization of mammalian selenoproteomes. Science 300, 1439–1443. [PubMed: 12775843]

Kung JE, and Jura N (2016). Structural Basis for the Non-catalytic Functions of Protein Kinases. Structure 24, 7–24. [PubMed: 26745528]

Labunskyy VM, Hatfield DL, and Gladyshev VN (2014). Selenoproteins: molecular pathways and physiological roles. Physiol Rev 94, 739–777. [PubMed: 24987004]

Longtine MS, McKenzie A 3rd, Demarini DJ, Shah NG, Wach A, Brachat A, Philippsen P, and Pringle JR (1998). Additional modules for versatile and economical PCR-based gene deletion and modification in Saccharomyces cerevisiae. Yeast 14, 953–961. [PubMed: 9717241]

Luikenhuis S, Perrone G, Dawes IW, and Grant CM (1998). The yeast Saccharomyces cerevisiae contains two glutaredoxin genes that are required for protection against reactive oxygen species. Mol Biol Cell 9, 1081–1091. [PubMed: 9571241]

Luong P, Kinch LN, Brautigam CA, Grishin NV, Tomchick DR, and Orth K (2010). Kinetic and structural insights into the mechanism of AMPylation by VopS Fic domain. J Biol Chem 285, 20155–20163. [PubMed: 20410310]

Madej T, Lanczycki CJ, Zhang D, Thiessen PA, Geer RC, Marchler-Bauer A, and Bryant SH (2014). MMDB and VAST+: tracking structural similarities between macromolecular complexes. Nucleic Acids Res 42, D297–303. [PubMed: 24319143]

Manning G, Whyte DB, Martinez R, Hunter T, and Sudarsanam S (2002). The protein kinase complement of the human genome. Science 298, 1912–1934. [PubMed: 12471243]

McLain AL, Szweda PA, and Szweda LI (2011). alpha-Ketoglutarate dehydrogenase: a mitochondrial redox sensor. Free Radic Res 45, 29–36. [PubMed: 21110783]

Mieyal JJ, and Chock PB (2012). Posttranslational modification of cysteine in redox signaling and oxidative stress: Focus on s-glutathionylation. Antioxid Redox Signal 16, 471–475. [PubMed: 22136616]

Min X, Lee BH, Cobb MH, and Goldsmith EJ (2004). Crystal structure of the kinase domain of WNK1, a kinase that causes a hereditary form of hypertension. Structure 12, 1303–1311. [PubMed: 15242606]

Minor W, Cymborowski M, Otwinowski Z, and Chruszcz M (2006). HKL-3000: the integration of data reduction and structure solution--from diffraction images to an initial model in minutes. Acta Crystallogr D Biol Crystallogr 62, 859–866. [PubMed: 16855301]

Muller MP, Peters H, Blumer J, Blankenfeldt W, Goody RS, and Itzen A (2010). The Legionella effector protein DrrA AMPylates the membrane traffic regulator Rab1b. Science 329, 946–949. [PubMed: 20651120]

Neal SE, Dabir DV, Tienson HL, Horn DM, Glaeser K, Ogozalek Loo RR, Barrientos A, and Koehler CM (2015). Mia40 Protein Serves as an Electron Sink in the Mia40-Erv1 Import Pathway. J Biol Chem 290, 20804–20814. [PubMed: 26085103]

Nguyen KB, Sreelatha A, Durrant ES, Lopez-Garrido J, Muszewska A, Dudkiewicz M, Grynberg M, Yee S, Pogliano K, Tomchick DR, et al. (2016). Phosphorylation of spore coat proteins by a family of atypical protein kinases. Proc Natl Acad Sci U S A 113, E3482–3491. [PubMed: 27185916]

Otwinowski Z, Borek D, Majewski W, and Minor W (2003). Multiparametric scaling of diffraction intensities. Acta Crystallogr A 59, 228–234. [PubMed: 12714773]

Rak M, Tetaud E, Godard F, Sagot I, Salin B, Duvezin-Caubet S, Slonimski PP, Rytka J, and di Rago JP (2007). Yeast cells lacking the mitochondrial gene encoding the ATP synthase subunit 6 exhibit a selective loss of complex IV and unusual mitochondrial morphology. J Biol Chem 282, 10853–10864. [PubMed: 17261589]

Roux KJ, Kim DI, and Burke B (2013). BioID: a screen for protein-protein interactions. Curr Protoc Protein Sci 74, Unit 19 23.

Saaranen MJ, Salo KE, Latva-Ranta MK, Kinnula VL, and Ruddock LW (2009). The C-terminal active site cysteine of Escherichia coli glutaredoxin 1 determines the glutathione specificity of the second step of peptide deglutathionylation. Antioxid Redox Signal 11, 1819–1828. [PubMed: 19361272]

Salomon D, Guo Y, Kinch LN, Grishin NV, Gardner KH, and Orth K (2013). Effectors of animal and plant pathogens use a common domain to bind host phosphoinositides. Nat Commun 4, 2973. [PubMed: 24346350]

Salomon D, and Sessa G (2010). Identification of growth inhibition phenotypes induced by expression of bacterial type III effectors in yeast. J Vis Exp.

Schrodinger LLC (2015). The PyMOL Molecular Graphics System, Version 1.8.

Shelton MD, Chock PB, and Mieyal JJ (2005). Glutaredoxin: role in reversible protein s-glutathionylation and regulation of redox signal transduction and protein translocation. Antioxid Redox Signal 7, 348–366. [PubMed: 15706083]

Shi F, Telesco SE, Liu Y, Radhakrishnan R, and Lemmon MA (2010). ErbB3/HER3 intracellular domain is competent to bind ATP and catalyze autophosphorylation. Proc Natl Acad Sci U S A 107, 7692–7697. [PubMed: 20351256]

Stadtman TC (1974). Selenium biochemistry. Science 183, 915–922. [PubMed: 4605100]

Sun R, Eriksson S, and Wang L (2012). Oxidative stress induced S-glutathionylation and proteolytic degradation of mitochondrial thymidine kinase 2. J Biol Chem 287, 24304–24312. [PubMed: 22661713]

Tagliabracci VS, Engel JL, Wen J, Wiley SE, Worby CA, Kinch LN, Xiao J, Grishin NV, and Dixon JE (2012). Secreted kinase phosphorylates extracellular proteins that regulate biomineralization. Science 336, 1150–1153. [PubMed: 22582013]

Tagliabracci VS, Wiley SE, Guo X, Kinch LN, Durrant E, Wen J, Xiao J, Cui J, Nguyen KB, Engel JL, et al. (2015). A Single Kinase Generates the Majority of the Secreted Phosphoproteome. Cell 161, 1619–1632. [PubMed: 26091039]

Takeda K, Cabrera M, Rohde J, Bausch D, Jensen ON, and Ungermann C (2008). The vacuolar V1/V0-ATPase is involved in the release of the HOPS subunit Vps41 from vacuoles, vacuole fragmentation and fusion. FEBS Lett 582, 1558–1563. [PubMed: 18405665]

Taylor SS, and Kornev AP (2011). Protein kinases: evolution of dynamic regulatory proteins. Trends Biochem Sci 36, 65–77. [PubMed: 20971646]

Taylor SS, Shaw A, Hu J, Meharena HS, and Kornev A (2013). Pseudokinases from a structural perspective. Biochemical Society transactions 41, 981–986. [PubMed: 23863167]

Tu BP, Kudlicki A, Rowicka M, and McKnight SL (2005). Logic of the yeast metabolic cycle: temporal compartmentalization of cellular processes. Science 310, 1152–1158. [PubMed: 16254148]

Wagner T, Bellinzoni M, Wehenkel A, O'Hare HM, and Alzari PM (2011). Functional plasticity and allosteric regulation of alpha-ketoglutarate decarboxylase in central mycobacterial metabolism. Chem Biol 18, 1011–1020. [PubMed: 21867916]

Wollweber L (1990). Harlow E and Lane D (Editors), Antibodies: A Laboratory Manual. XIII + 726 S., 50 Abb., 62 Tab. Cold Spring Harbor 1988. Cold Spring Harbor Laboratory. $50.00. ISBN: 0–87969-314–2. Journal of Basic Microbiology 30, 164–164.

Xiao J, Worby CA, Mattoo S, Sankaran B, and Dixon JE (2010). Structural basis of Fic-mediated adenylylation. Nat Struct Mol Biol 17, 1004–1010. [PubMed: 20622875]

Zadzinski R, Fortuniak A, Bilinski T, Grey M, and Bartosz G (1998). Menadione toxicity in Saccharomyces cerevisiae cells: activation by conjugation with glutathione. Biochem Mol Biol Int 44, 747–759. [PubMed: 9584988]

Zeqiraj E, and van Aalten DM (2010). Pseudokinases-remnants of evolution or key allosteric regulators? Curr Opin Struct Biol 20, 772–781. [PubMed: 21074407]

Zhu Q, Venzke D, Walimbe AS, Anderson ME, Fu Q, Kinch LN, Wang W, Chen X, Grishin NV, Huang N, et al. (2016). Structure of protein O-mannose kinase reveals a unique active site architecture. eLife 5.

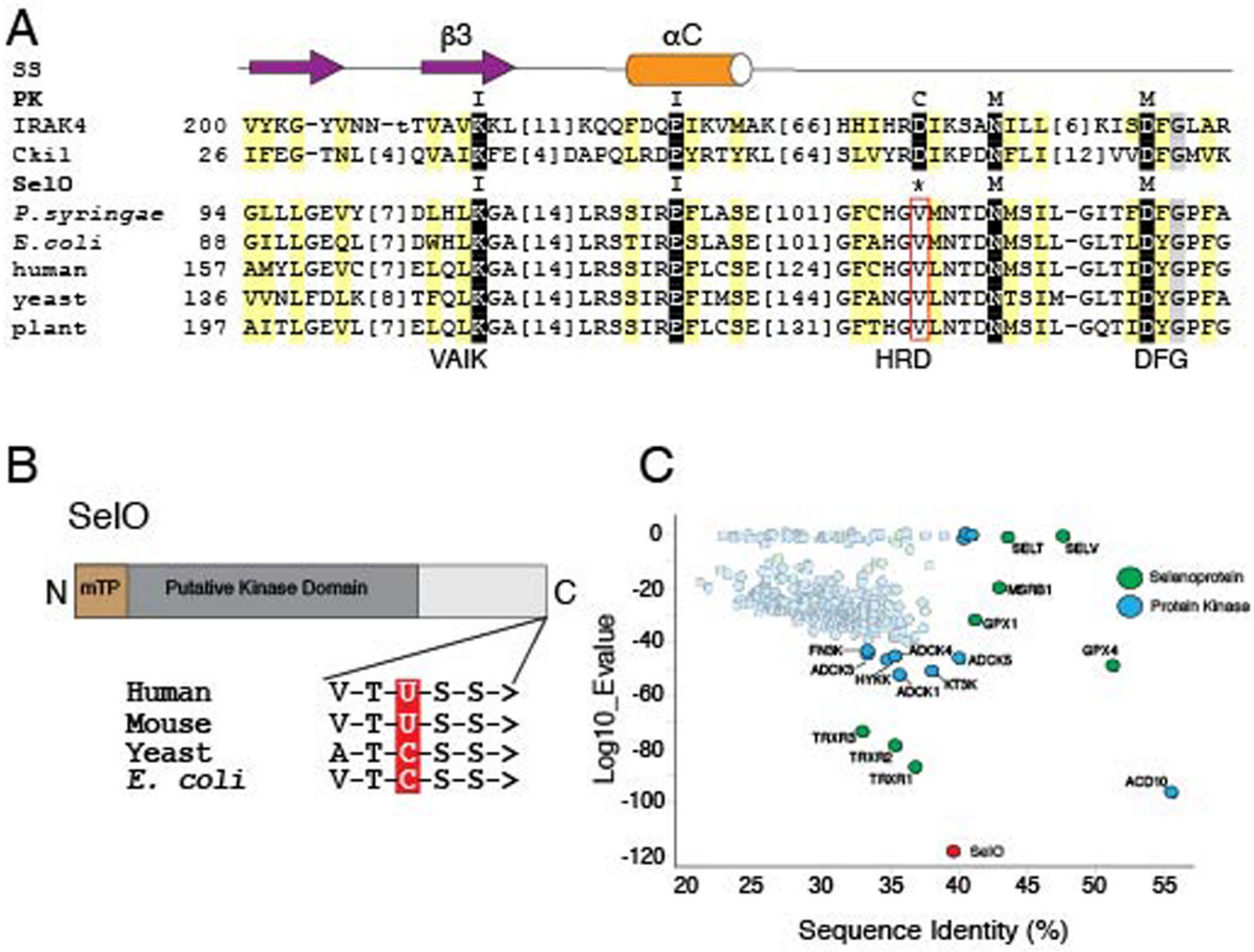

Figure 1. SelO is an evolutionarily conserved pseudokinase. (See also Figure S1)

(A) Multiple sequence alignment highlighting conserved active site residues in the SelO pseudokinases. Conserved positions in SelO and protein kinases (PK) are highlighted yellow (hydrophobic) and gray (small). Conserved catalytic motif residues are highlighted black and labeled above: ion pair (I; VAIK), catalytic (C, HRD) and Mg^{2+}-binding (M, DFG). Starting residue numbers are indicated before the alignment, with omitted residue numbers in brackets. Secondary structure (SS) elements are indicated above the alignment as arrow (strand) and cylinder (helix). Cki1, *S. pombe* protein kinase CK1; IRAK4, human interleukin-1 receptor-associated kinase 4.

(B) Schematic representation of the SelO protein depicting the predicted mitochondrial targeting peptide (mTP) and kinase domain. The amino acid sequences at the C-terminus of the human, mouse, yeast and *E. coli* proteins are shown, highlighting the Sec (U) in the human and mouse proteins and Cys (C) in the yeast and *E. coli* proteins. > denotes the C-terminus.

(C) BLAST analysis depicting the closest bacterial homologs retrieved from a search using the human protein kinases (blue) and selenoproteins (green) as queries. SelO is in red.

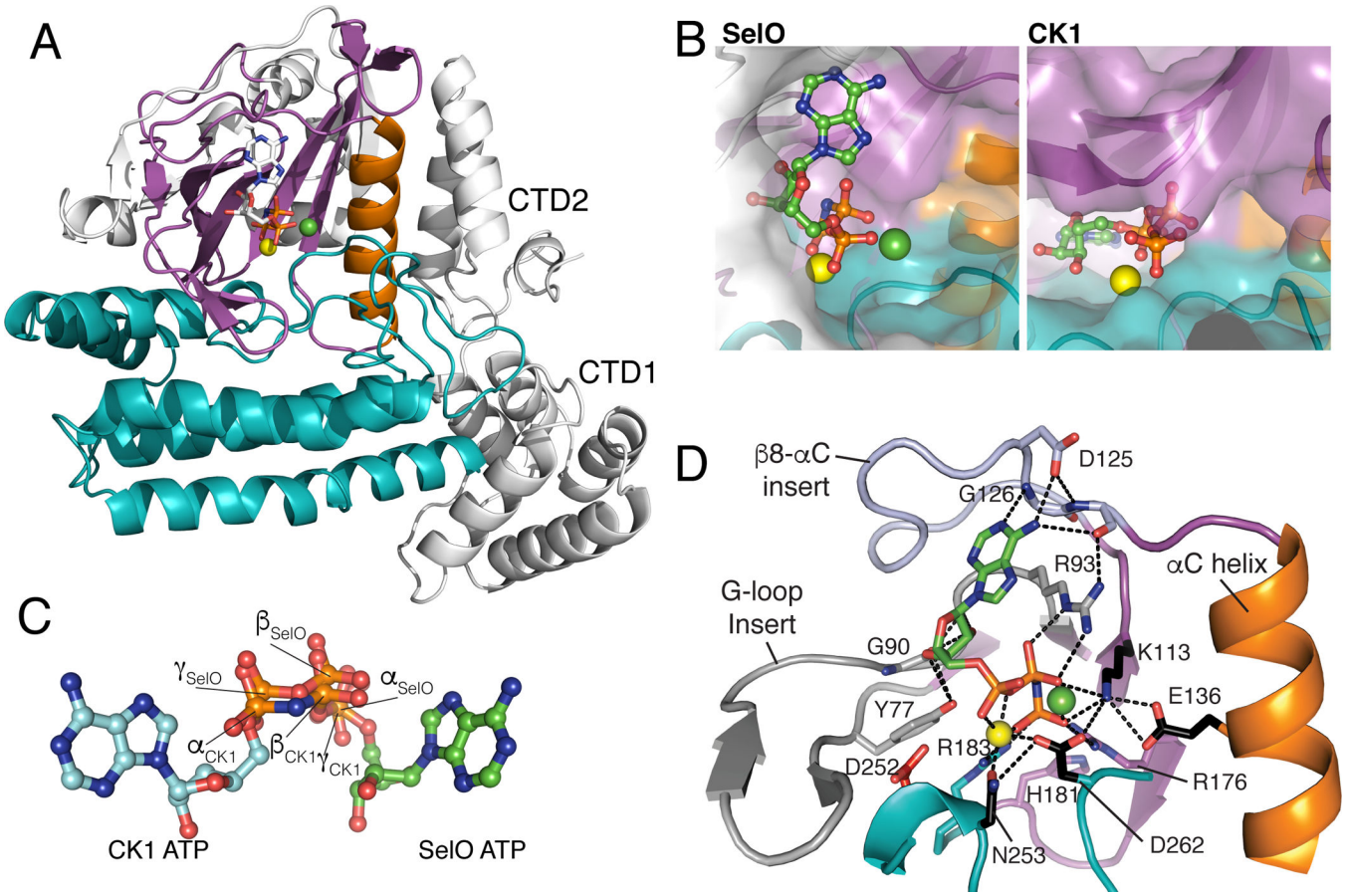

Figure 2. The crystal structure of *P. syringae* SelO reveals an atypical protein kinase fold with ATP flipped in the active site. (See also Figure S2 & Table S1)

(A) Ribbon representation of *P. syringae* SelO. The N- and C-lobes are shown in magenta and teal, respectively. The αC helix is in orange. The N-terminal extension and C-terminal domains are in white. The AMP-PNP is shown in stick representation and the Mg^{2+} and Ca^{2+} ions are shown as yellow and green spheres, respectively.

(B) Surface representations illustrating the orientation of the nucleotide in the active site of *P. syringae* SelO (left), colored as above, but with N-lobe insertions shown in white, and protein kinase CK1 (right, pdb: 1csn) in the same orientation as SelO.

(C) Ball-and-stick representation of SelO and CK1 nucleotides superimposed as a result of superposition of the proteins. The α, β, and γ phosphates of SelO and CK1 are highlighted.

(D) Enlarged image of the nucleotide-binding pocket of *P. syringae* SelO highlighting the flipped ATP binding pocket. Two unique SelO insertions bind the flipped nucleotide, including a G90 and Y77 from the elongated G-loop (gray) that form hydrogen bonds (black dotted lines) with the ribose ring and R93 that forms hydrogen bonds with the β-phosphate, as well as D125 and G126 from the β8-αC insert (light blue) forming hydrogen bonds with the nucleotide. Two Arg sidechains (R176 and R183) form a unique charged pocket for the γ-phosphate, with the sidechains from R183 and H181 replacing the canonical ATP nucleotide binding site.

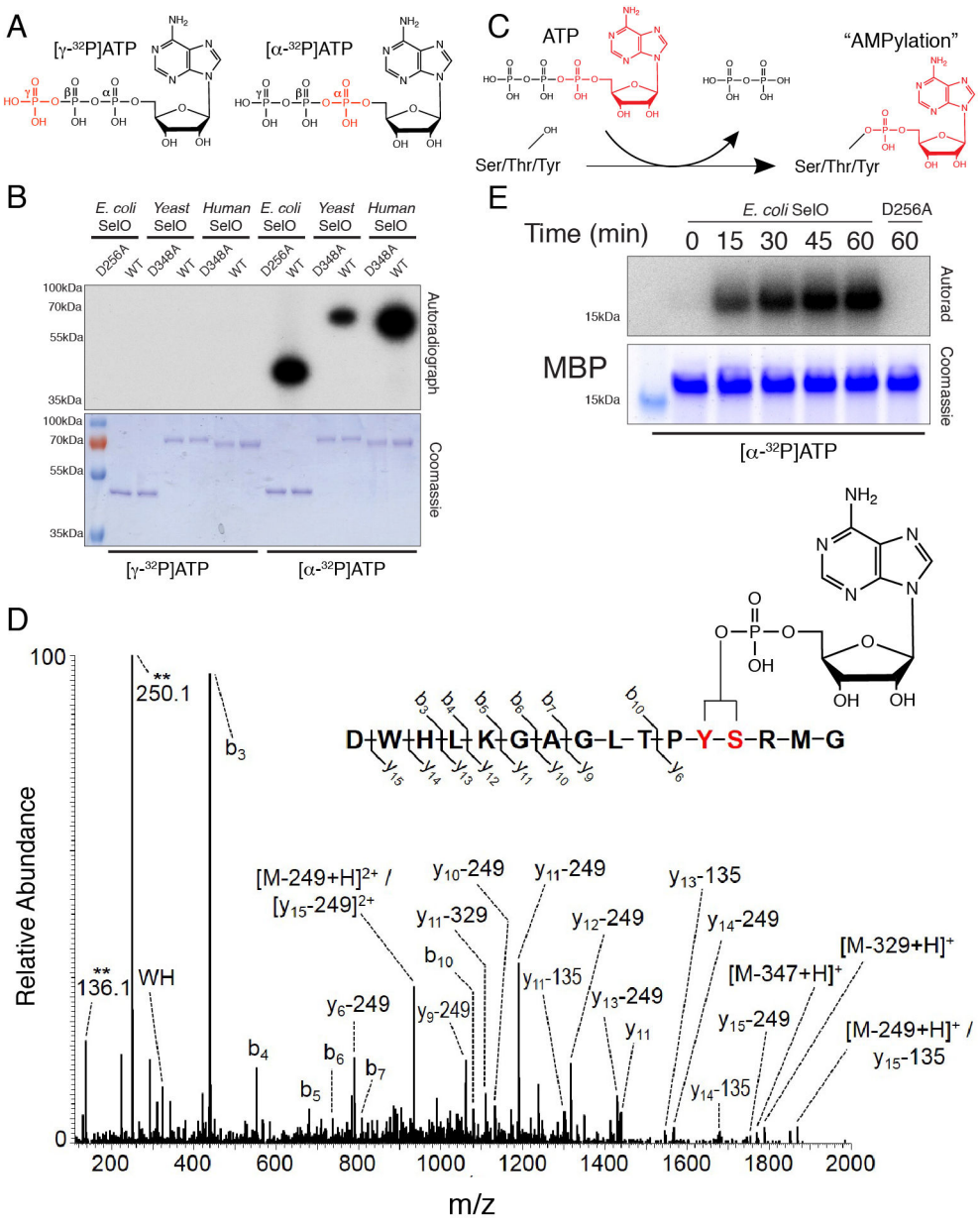

Figure 3. SelO pseudokinases AMPylate protein substrates. (See also Figure S3)

(A) Structure of the ATP molecule highlighting the position of the ^{32}P on the γ-phosphate (left) or α-phosphate (right) in red.

(B) Autoradiograph depicting the incorporation of **γ**$^{-32}$P from [**γ**$^{-32}$P]ATP (left) or α^{-32}P from [α^{-32}P]ATP (right) using *E. coli*, *S. cerevisiae* and human SelO (U667C), or catalytically inactive mutants. Reaction products were resolved by SDS-PAGE and visualized by Coomassie blue staining (lower) and autoradiography (upper).

(C) Proposed reaction catalyzed by the SelO pseudokinases.

(D) MS/MS spectrum of an AMPylated *E. coli* SelO peptide ion. The precursor ion, *m/z* 1059.47 (2+), of the AMPylated peptide was subjected to HCD fragmentation to generate the spectrum shown. Fragment ions containing the modified residue show characteristic

mass shifts corresponding to loss of the AMP group (−329, −249, and −135 Da). Unique ions corresponding to neutral loss of the AMP group (labeled with **) are present at 136.1 and 250.1 Da. Location of the AMP group on the peptide can be localized to either the tyrosine or serine residue highlighted in red.

(E) Time dependent incorporation of α-^{32}P from [α-^{32}P]ATP into MBP by SelO or SelO D256A. Reaction products were analyzed as in (B).

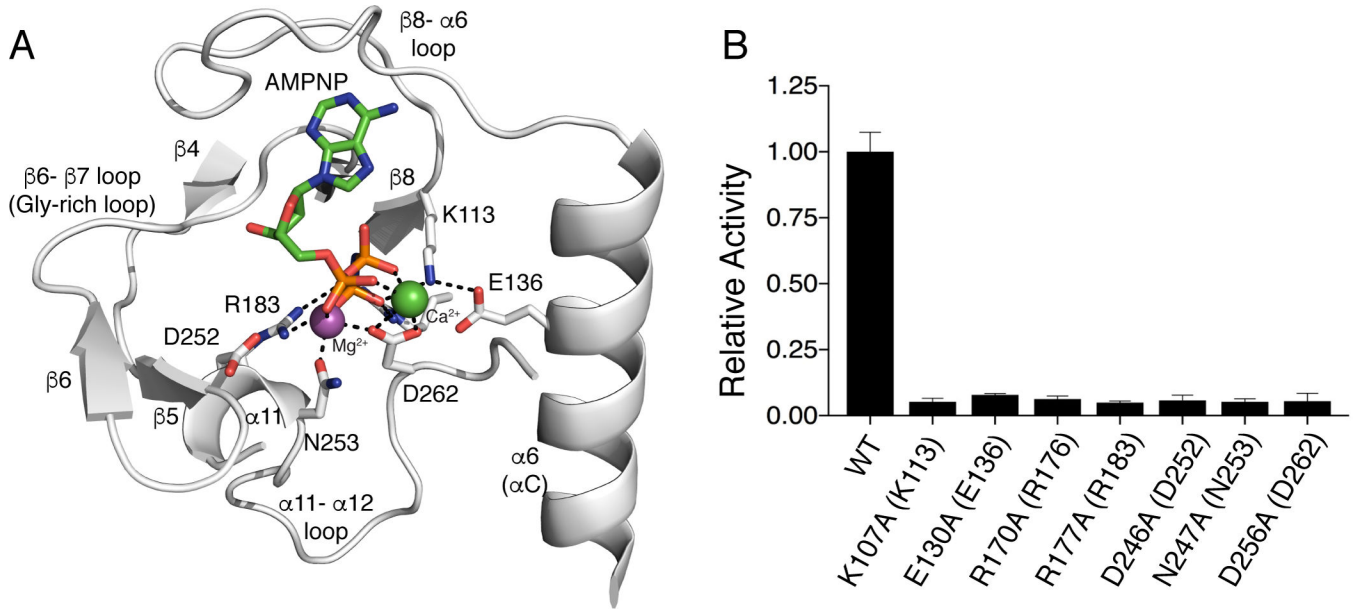

Figure 4. A unique active site architecture in *P. syringae* SelO facilitates ATP binding and AMPylation activity. (See also Figure S7).

(A) Enlarged image of the nucleotide-binding pocket of *P. syringae* SelO showing the detailed molecular interactions important for nucleotide binding and catalysis. Interactions are shown as dashed lines. The AMP-PNP molecule is shown in stick and the Mg^{2+} and Ca^{2+} ions are shown as purple and green spheres, respectively.

(B) Activity of *E. coli* SelO or active site mutants using MBP and [α−^{32}P]ATP as substrates. Reaction products were resolved by SDS-PAGE and radioactive gel bands were excised and quantified by scintillation counting. The numbering in parentheses corresponds to the residues in *P. syringae* SelO.

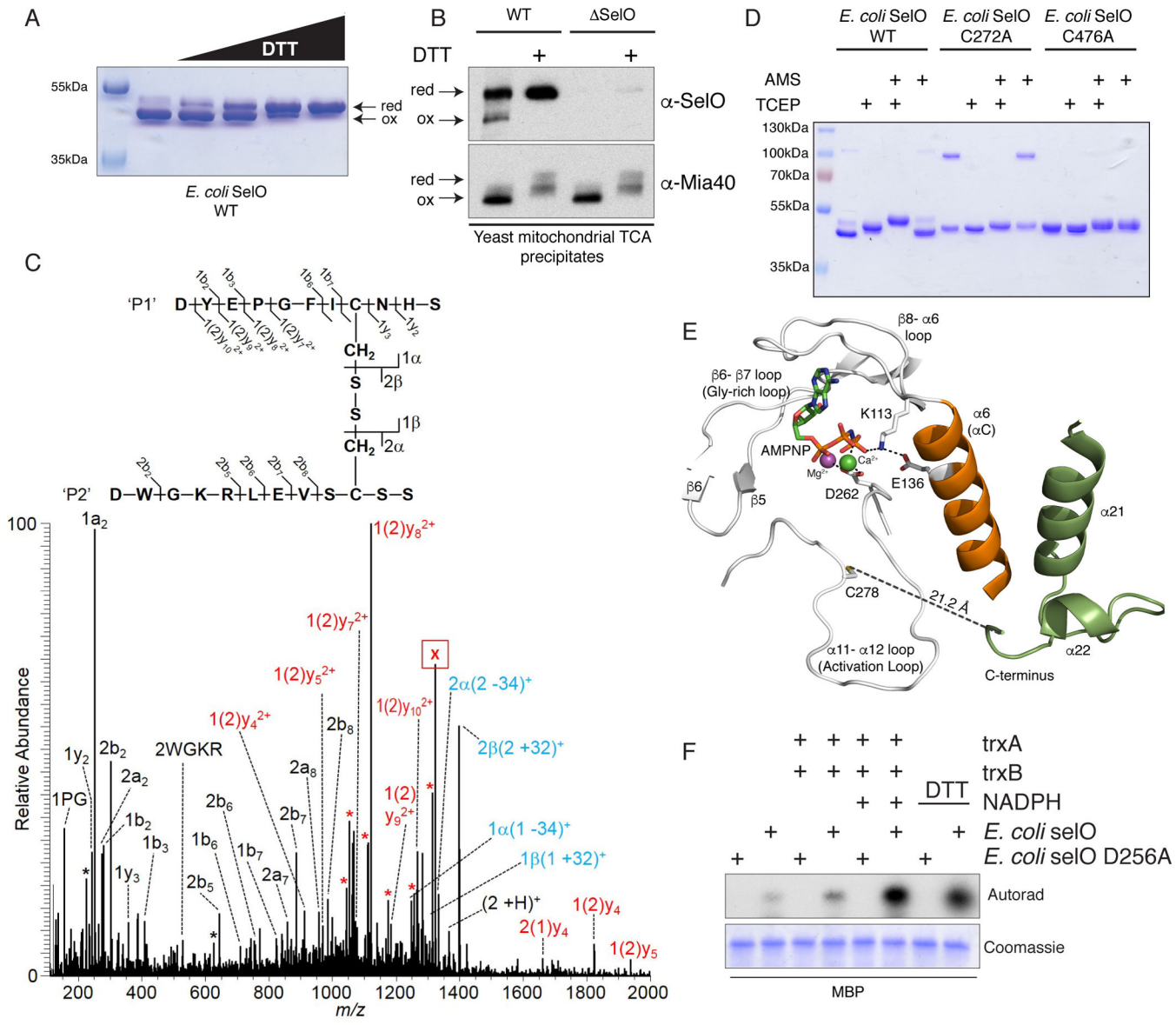

Figure 5. SelO activity is regulated by an intramolecular disulfide bridge. (See also Figure S4).

(A) Non-reducing SDS PAGE and Coomassie blue staining analysis of recombinant *E. coli* SelO purified in the absence of reducing agent and incubated with increasing concentrations of DTT (0 – 1mM).

(B) Non-reducing SDS PAGE and protein immunoblotting of yeast mitochondrial TCA precipitates depicting endogenous *S. cerevisiae* SelO and Mia40. TCA precipitates were treated with or without DTT prior to electrophoresis.

(C) MS/MS spectrum of *E. coli* SelO peptides linked by a disulfide bond: DYEPGFICNHS / DWGKRLEVSCSS. The precursor ion, *m/z* 1323.07 (2+) (labeled with "X"), was subjected to HCD fragmentation to generate the spectrum shown. Peaks labeled with an asterisk (*) correspond to neutral loss of ammonia (−17 Da) or water (−18 Da) from fragment ions. The peak labels are color coded depending on the status of the disulfide bond (SS) for that particular ion: black (no SS), red (intact SS), and blue (asymmetric cleavage of SS, α or β).

(D) Non-reducing SDS PAGE and Coomassie blue staining analysis of recombinant *E. coli* SelO or the C272A and C476A mutants purified under non-reducing conditions and incubated with the reducing agent TCEP or the alkylating agent AMS. The species at ~100kDa in the SelO C272A mutant is a dimer formed between two molecules of *E. coli* SelO linked by an intermolecular disulfide.

(E) Enlarged image of the active site highlighting the activation loop C278 (C272 in *E. coli* SelO) and the C-terminus of the protein. The α6 (αC equivalent) is in orange and the α21 and α22 helices are in green. The AMP-PNP molecule is shown in stick and the Mg^{2+} and Ca^{2+} ions are shown as purple and green spheres, respectively.

(F) Incorporation of ^{32}P AMP from [α−^{32}P]ATP by *E. coli* SelO or the D256A mutant under non-reducing or reducing conditions (DTT or the thioredoxin system). (trxA; *E. coli* thioredoxin, trxB; *E. coli* thioredoxin reductase). Reaction products were analyzed as in Figure 3B.

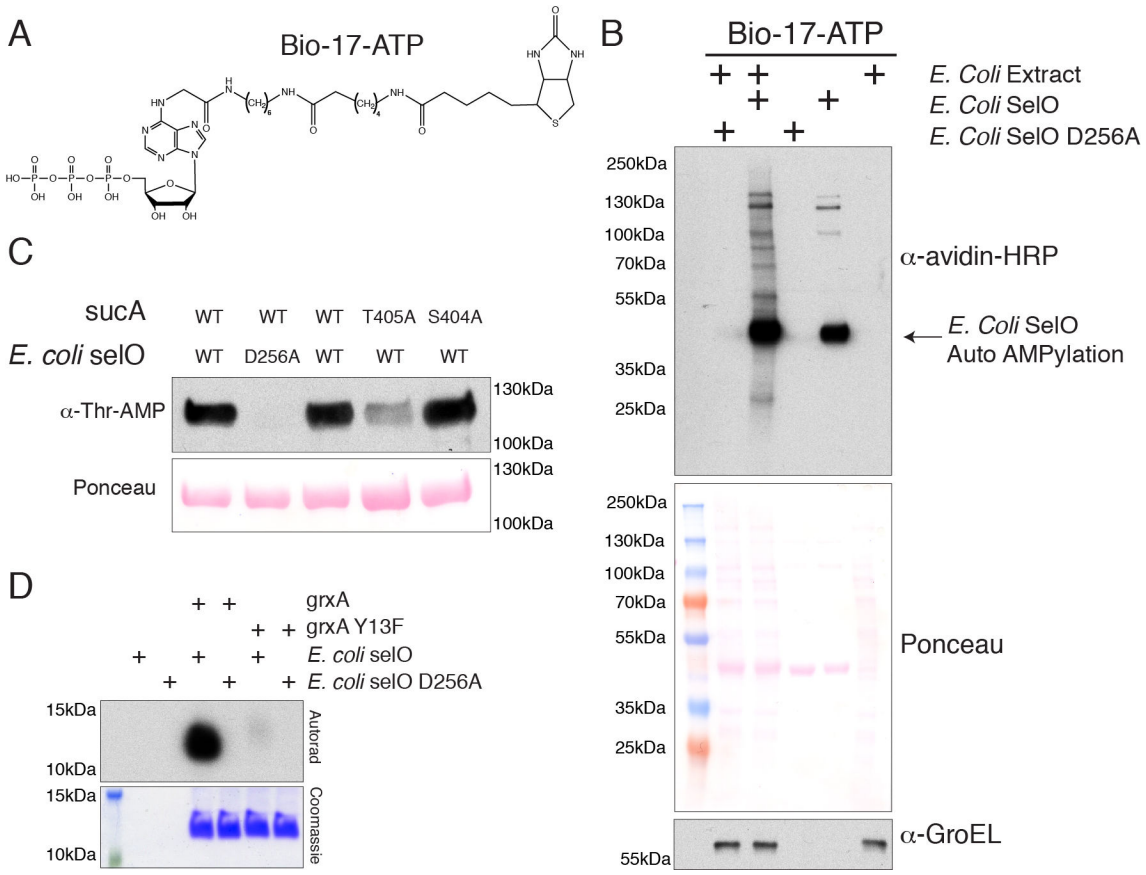

Figure 6. SelO AMPylates mitochondrial proteins. (See also Figure S5 & Table S2).

(A) Structure of biotin-17-ATP (bio-17-ATP) used in these experiments to identify SelO substrates.

(B) Representative blot using avidin-HRP to detect biotinylated proteins following incubation of *E. coli* extracts with bio-17-ATP and *E. coli* SelO or the D256A mutant. The Ponceau stained membrane and an immunoblot for GroEL are shown as loading controls.

(C) α-Thr AMP protein immunoblotting of Ni-NTA affinity purified His-tagged sucA (or mutants) from SelO KO *E.coli* extracts expressing untagged WT SelO or the inactive mutant. The Ponceau stained membrane is shown.

(D) Autoradiograph depicting the incorporation of $\alpha-^{32}$P AMP from [$\alpha-^{32}$P]ATP by *E. coli* SelO or the D256A mutant into *E. coli* grxA. Reaction products were analyzed as in Figure 3B.

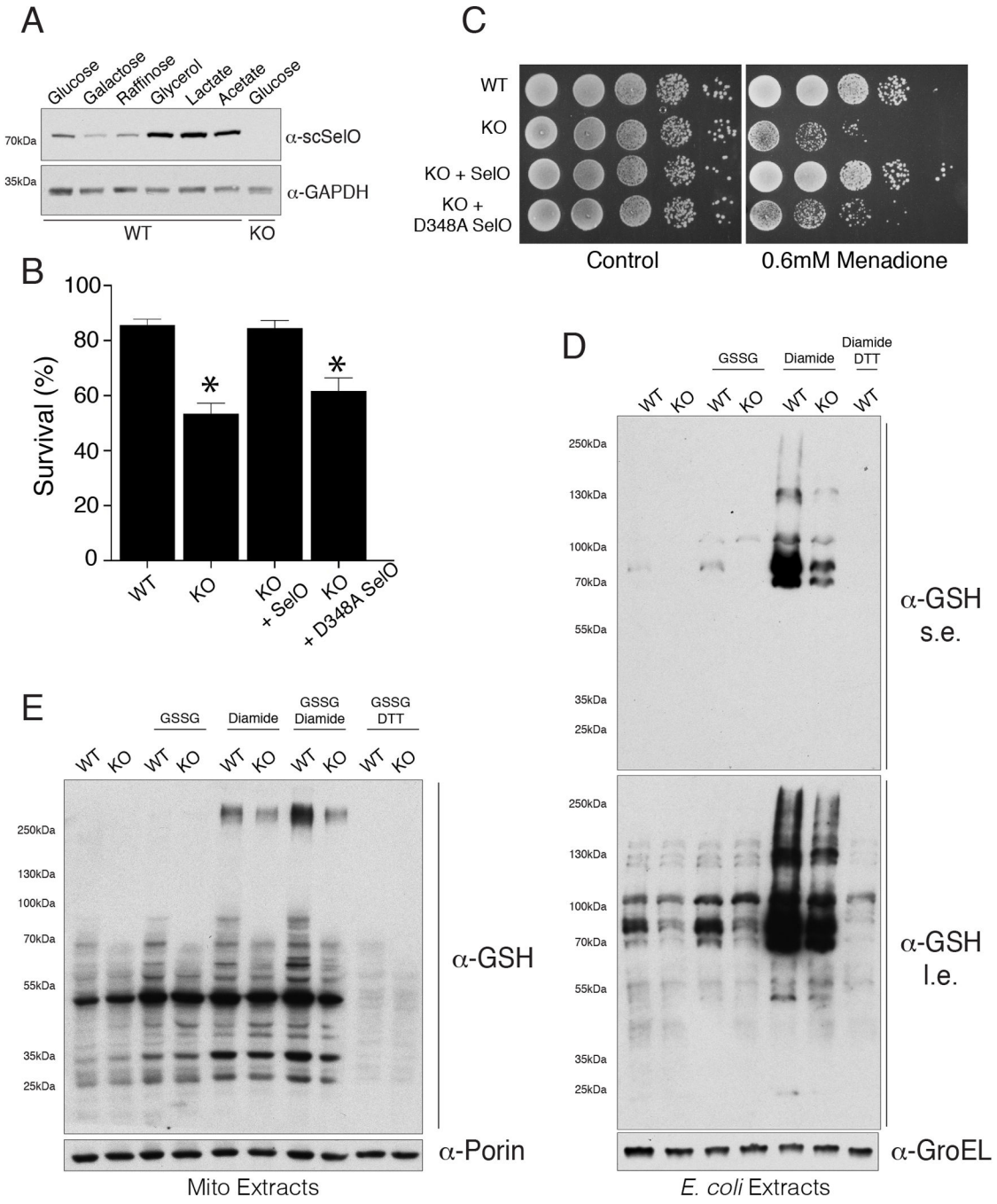

Figure 7. SelO protects yeast cells from oxidative stress and regulates protein S-glutathionylation. (See also Figure S6).

(A) Representative protein immunoblots of WT and SelO KO yeast cell extracts (strain MR6) grown in medium with the indicated carbon source. *S. cerevisiae* SelO (ScSelO) and GAPDH (loading control) are shown.

(B) Percent survival of *S. cerevisiae* (strain MR6) WT, SelO KO or SelO KO cells complemented with WT or D348A SelO following treatment with 100 μM H_2O_2 in glucose

minimal medium for 200 min at 28°C. Results represent the mean of 3 independent experiments. * $p < 0.005$ vs WT.

(C) Representative growth assays of *S. cerevisiae* (strain BY4741) untreated (left) or 0.6 mM menadione treated (right). WT, SelO KO or SelO KO complemented with WT or D348A SelO strains were analyzed.

(D) Representative protein immunoblots of WT and SelO KO *E. coli* extracts following treatment of intact cells with oxidized glutathione (GSSG) or diamide. Cells were also treated with diamide followed by DTT as a negative control. Extracts were probed with anti-glutathionylation (GSH) and *E. coli* GroEL (loading control). Results are representative of at least 3 independent experiments. s.e. (short exposure). l.e. (long exposure).

(E) Representative protein immunoblots of crude mitochondrial extracts isolated from WT and SelO KO *S. cerevisiae* (strain MR6) following treatment of intact mitochondria with oxidized glutathione (GSSG) and/or diamide. Mitochondria were also treated with GSSG followed by DTT as a negative control. Extracts were probed with anti-glutathionylation (GSH) and *S. cerevisiae* porin (loading control). Results are representative of at least 3 independent experiments.